CHALMERS
UNIVERSITY OF TECHNOLOGY

Fixation of Rotor Laminate in an Electric Machine

Remove the usage of liquid nitrogen during assembly and keeping a high manufacturability

Master's thesis in Applied Mechanics

Erik Nylander, Adam Olson

DEPARTMENT OF INDUSTRIAL AND MATERIALS SCIENCE

CHALMERS UNIVERSITY OF TECHNOLOGY
Gothenburg, Sweden 2022
www.chalmers.se

Master's thesis 2022

Fixation of Rotor Laminate in an Electric Machine

Remove the usage of liquid nitrogen during assembly and keeping a high manufacturability

Erik Nylander, Adam Olson

CHALMERS
UNIVERSITY OF TECHNOLOGY

Department of Industrial and Materials Science
Division of Material and Computational Mechanics
Chalmers University of Technology
Gothenburg, Sweden 2022

Fixation of Rotor Laminate in an Electric Machine

ERIK NYLANDER, ADAM OLSON

Supervisor: Jörgen Stefors, Volvo Cars
Examiner: Magnus Ekh, Division of Material and Computational Mechanics, Chalmers University of Technology

Master's Thesis 2022
Department of Industrial and Materials Science
Division of Material and Computational Mechanics
Chalmers University of Technology
SE-412 96 Gothenburg
Telephone +46 31 772 1000

Cover: An integrated drive unit XC90 T8 Twin Engine. Shaft, rotor, stator and stator housing is visible [1].

Typeset in LaTeX
Printed by Chalmers Reproservice
Gothenburg, Sweden 2022

Fixation of Rotor Laminate in an Electric Machine
Remove the usage of liquid nitrogen during assembly and keeping a high manufacturability
Erik Nylander, Adam Olson
Department of Industrial and Materials Science
Chalmers University of Technology

Abstract

In the future it is expected to exist twice as many cars on the roads as it does today. For companies manufacturing electric cars, such as Volvo Cars, hundreds of millions of traction motors must be produced. Therefore, an efficient and safe way of doing this is of great interest. Today, Volvo Cars assembles the rotor onto the shaft using a shrink-fit method where the rotor stack is heated and the shaft is cooled using liquid nitrogen. A new solution that can achieve the requests on the motor without using liquid nitrogen as cooling would simplify the assembly process, make it safer, and reduce the manufacturing costs.

Alternative geometries to the regular circular shaft and rotor were investigated in this work by creating models using ANSA and analysing them with Abaqus. The geometry of the interference between shaft and rotor that was produced from this investigation is called valleys. It is based from the already existing shaft, but with circular cutouts around the outer edge. The cutouts are supposed to match a grinding tool to obtain a high manufacturability. The chosen solution was optimized against torque capacity, slip angle and fatigue life.

The design is not final since the model has not yet been tested with any temperature gradient across the assemble, which may affect the contact between rotor and shaft. Real life testing is also necessary to ensure that the simulations are resembling the reality.

Keywords: Shrink fit, rotor, Laminate, Electric machine, Grip, Torque, Slip, Car, Finite element method.

Acknowledgements

First of all, we would like to thank Volvo Cars for giving us the opportunity to perform an interesting and rewarding Master's thesis at the Electric Driveline department. We have gained great knowledge about finite element analysis and how engineering work is carried out at a company.

Secondly, we would like to give our supervisor at Volvo, Jörgen Stefors, a big thank you for supporting the project and providing us with necessary information and teaching us how to use the different softwares. Also, special thanks goes to Joakim Ehn at Volvo who was of great help with the design process during the project.

Finally, our examiner at Chalmers, Magnus Ekh, deserves a big thanks for providing feedback and constructive criticism towards the project, helping us creating a well-composed report.

Erik Nylander & Adam Olson
Gothenburg, June 2022

Nomenclature

Parameters

E_r	Young's modulus, rotor
E_s	Young's modulus, shaft
$d_{r,i}$	Inner diameter of rotor
$d_{r,o}$	Outer diameter of rotor
$d_{s,i}$	Inner diameter of shaft
$d_{s,o}$	Outer diameter of shaft
F_c	Centrifugal force
i	Index inner diameter
m	Mass
M	Transferable moment
o	Index outer diameter
p	Contact pressure
r	Index rotor
$r_{r,i}$	Inner radius of rotor
$r_{r,o}$	Outer radius of rotor
$r_{s,i}$	Inner radius of shaft
$r_{s,o}$	Outer radius of shaft
R	Radius
s	Index shaft
t	Thickness of one laminate
T_r	Temperature increase, rotor
T_s	Temperature decrease, shaft
u_r	Displacement of rotor due to centrifugal force
u_s	Displacement of shaft due to centrifugal force
α_r	Coefficient of thermal expansion, rotor

α_s	Coefficient of thermal expansion, shaft
β	Slip angle between shaft and rotor
Δ	Stationary diametric grip
Δ_{rot}	Diametric grip as function of rotational velocity
κ_r	The ratio $d_{r,i}/d_{r,o}$
κ_s	The ratio $d_{s,i}/d_{s,o}$
μ	Friction coefficient between rotor and shaft
ν_r	Poisson's ratio, rotor
ν_s	Poisson's ratio, shaft
ρ_r	Density of the rotor material
ρ_s	Density of the shaft material
ω	Rotational velocity

Contents

1
Introduction

It is expected to be over two billion vehicles globally by the year 2035. Having a part of them electrified results in hundreds of millions of traction motors in the range of 50-500 kW needing to be produced. Consequently, it is of vital importance to design and produce them efficiently [2]. Previous benchmark analysis has shown that for high RPM and torque, a key and keyway is the most common solution to fasten the rotor to the shaft. However, it adds complexity to the assembly of the shaft and rotor stack. Therefore alternative fixation solutions needs to be evaluated.

1.1 Background

A rotating electric machine is a device that converts electrical energy to rotational mechanical energy or vice versa. The main parts of the machine are the rotor, stator, and shaft, where the rotor is made of many thin laminates pressed together, see Figure 1.1. Rotational torque is transmitted to the rotor by an interaction in magnetic fields of the rotor and stator. The rotor, which is attached to the shaft, transfers the rotational energy out to the vehicle's wheels propelling it forward [3].

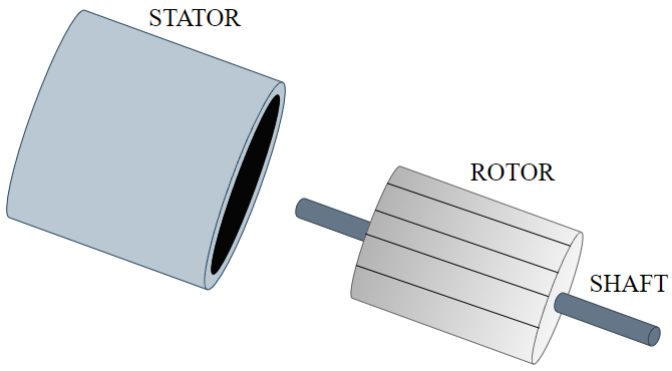

Figure 1.1: Schematic image of stator, rotor and shaft. The rotor is made up of thin laminates.

There are mainly two different types of electric machines used in electric vehicles, induction machines and permanent magnet synchronous machines (PMSM). In a PMSM, the electrical energy creates a rotating magnetic field in the stator, which the permanent magnets in the rotor follow [3]. The rotor is fixated to the shaft and transfers the rotation through a final drive to the wheels. The position of the shaft

is measured to provide the correct input to the stator. It is therefore important to make sure that the rotor is not slipping on the shaft, which change the stator's input and lower the efficiency of the machine.

The rotor consists of sub-stacks of laminates and magnets. Each sub-stack has about 100 press-joined laminates with a thickness under 1mm. Figure 1.2 shows a laminate with the magnets and a shaft. The magnets are inserted into the slots close to the laminates outer edge and the shaft is positioned into the center of the laminate. The cutouts surrounding the center hole decrease the weight and change the way the stresses spread throughout the laminate.

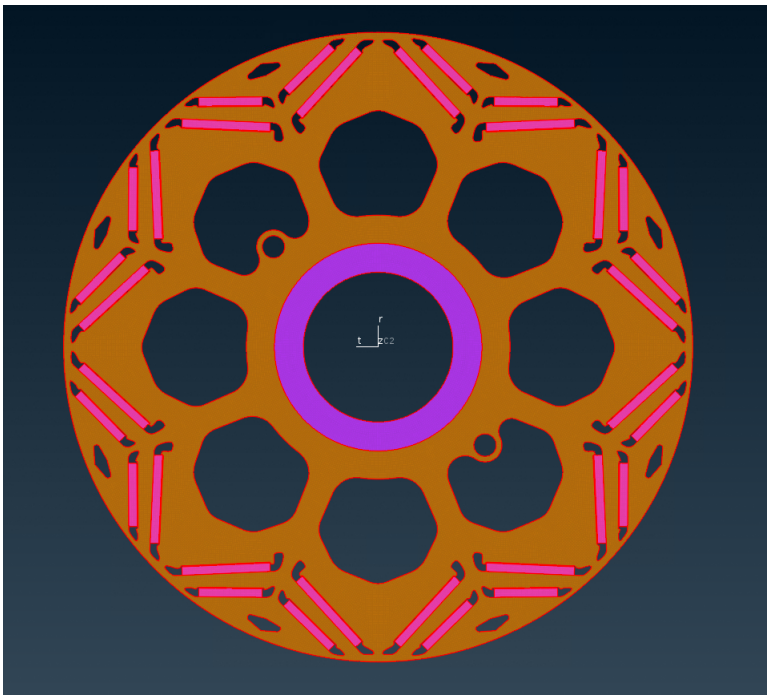

Figure 1.2: Cross section view of laminate, (brown), shrink fitted on to shaft, (purple), with inserted magnets, (pink). The open areas in the laminate exists to reduce weight and change stress paths.

The rotor is usually attached to the shaft with a key joint which reduces the chance of slippage between rotor and shaft but creates more intricate manufacturing- and assembly processes. Solutions with shrink-fits also occurs but with a greater risk of slippage. The rotor might even completely come loose from the shaft at the highest velocities, which has to be prevented. Hence, a solution which does not involve a key joint, assures no slippage and simplifies the shrink fit assembly process is sought after. Today at Volvo Cars, the rotor is attached to the shaft with a shrink fit.

1.1.1 Current solutions

Previous analysis has shown that using a key and keyway is the most common solution to attach the rotor to the shaft in an electric machine used in a vehicle,

see Figure 1.3. The key increases the transferable torque without slippage between shaft and rotor. The keyways are located on the shaft and the keys on the laminates to keep the parts together. Various electric machines have different number of keys, for example, in Tesla model S 60, only one key is used and in Toyota Prius 2003 four keys are used. The keyways are cutouts in the shaft, which results in stress concentrations. More keyways will therefore reduce the strength and fatigue life of the shaft. Therefore the trend is to reduce the number of keys [4]. Another drawback is that the key must be axially positioned and fixed, which adds complexity to the assembly. The key is fixated with a shrink-fit. The shaft is cooled down, making the key-way narrow, and the laminate is heated up, expanding the key. As a result, the key is hard to position or can become loose.

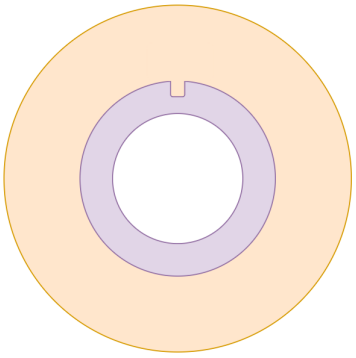

Figure 1.3: Schematic image showing a key and key-way locking mechanism.

Another solution is to remove all keys and instead use an interference fit like in the 2016 Audi A3 e-tron. The benefits of this method are that the diameter of the shaft can be reduced and the assembling process is more straightforward [5]. This method uses interference between the shafts outer diameter and the rotors inner diameter, creating pressure and a friction force which keep the rotor in place. A problem with this solution is that the pressure needs to be significant to keep the rotor in place, which can damage the rotor. Temperature variations during driving also have an impact. The expansion of the rotor will reduce the pressure between rotor and shaft.

1.2 Goal

The goal of this Master's thesis is to investigate if a non-circular shaft and laminate geometry is possible to shrink fit together without using liquid nitrogen, while maintaining a high manufacturability and meet the requirements on torque, stress and efficiency.

1.2.1 Specification

Removing the usage of liquid nitrogen during assembly decreases the temperature difference, and thereby the interference between rotor and shaft. Liquid nitrogen usually cools the shaft down to -150°C but for the sought solution, the cooling will

be limited to -40° C. The manufacturing tolerances for shaft and laminate have to be regarded to ensure that the worst-case still meets the requirements and is possible to assemble. The geometry must also be manufactured within reasonable manufacturing possibilities. To not lose efficiency in the electric machine, the relative angle between shaft and rotor has to be minimized and needs to be below 0.7°. The angle increase due to slippage between the parts at high torques or high rotational velocities. In addition, the solution also has to withstand shock loads in torque around 500Nm at highest velocities. The stresses should not exceed the yield limit of 421MPa. Easy manufacturing is highly valued, hence the solution will be embossed by this.

1.2.2 Deliverables

To accomplish the goal and solve the issues, the following deliverables need to be completed.

- Literature study on different fixation methods for the rotor and shaft assembly.
- Create an analytical estimation of transferable torque and contact pressure at alternating rotational velocities.
- Create a base case from previously made experiments to compare with.
- Evaluate simplified geometries to find one solution to develop further.
- The chosen geometry is optimized from a more complex model by using the existing laminate with magnets and also consider fatigue life.
- Design for a test plan for further investigation of the final solution.

1.2.3 Limitations

To complete the deliverables within the given time and the given resources, limitations were made. The complexity of the simulations is reduced by only considering one laminate. Hence, a 2D-models are used with the assumption of a plane stress case. The type of interference considered will be a shrink fit without any axial loading. The shrink-fit solution will be assumed to not affect the surface roughness, hence the friction coefficient will be constant along with other material properties. Only the innermost edge geometry of the laminate will be redesigned.

2
Analytical Solution

An analytical solution to a simplified geometry is here exploited to create a foundation on which the further simulations are based. Relevant theory for shrink-fitting, torque and contact pressure is described. The chapter will also present results in terms of contact pressure and transferable torque and how they vary with rotational velocity.

2.1 Theory

There are mainly two types of interference fit, press- and shrink fits. These types fulfill the same function but are carried out in different ways. The press-fit works by using force to press the shaft into the rotor. The parts are then fixed together due to the friction caused by their contact. The shrink fit is done by heating the rotor and cooling the shaft, leading to expansion and contraction respectively. The parts can then be fitted together without any force. When the assembly reaches room temperature, the parts will be held together by the interference between rotor and shaft in the same way as the press fit method [6]. The most dominant parameter in an interference fit is the grip, but the diameter also affects the connection [7].

The calculations below are done on one 0.27mm thick laminate without considering axial loading, and hence a plane stress case is assumed. The geometry and notations of the radii used for the analytical solution are seen in Figure 2.1. No magnets or cutouts in the laminate are regarded here and the cross section is completely circular.

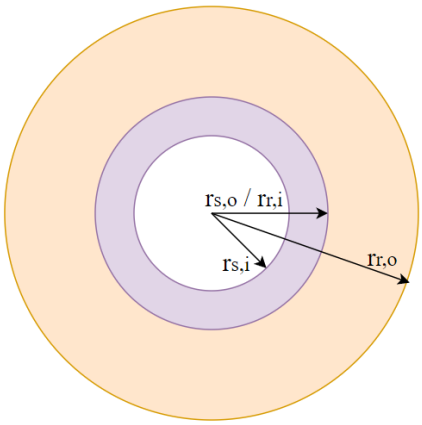

Figure 2.1: The geometry for which the analytical solution is obtained. The definition of the different radii is also shown.

2.1.1 Shrink fit

A shrink fit is achieved using temperature differences, where thermal expansion makes it possible to assemble the two parts. The required temperature difference for a known diametric grip Δ can be determined from the following equation

$$(\alpha_r T_r + \alpha_s T_s)\, d_{r,i} > \Delta \quad \text{with} \quad T_r \geq 0,\, T_s \leq 0 \tag{2.1}$$

where α is the coefficient of thermal expansion, $d_{r,i}$ is the inner diameter of the rotor and T is the increased/decreased temperature. The index r and s refers to *rotor* and *shaft* [8].

The contact pressure which occurs between the two parts due to the grip is determined as

$$p = \Delta \Bigg/ d_{r,i} \left[\frac{1}{E_r} \left(\frac{1+\kappa_r^2}{1-\kappa_r^2} + \nu_r \right) + \frac{1}{E_s} \left(\frac{1+\kappa_s^2}{1-\kappa_s^2} + \nu_s \right) \right] \tag{2.2}$$

where E is the Young's modulus, ν the Poisson's ratio, $\kappa_r = d_{r,i}/d_{r,o}$, $\kappa_s = d_{s,i}/d_{s,o}$ with index i and o refers to *inner* and *outer* diameters [9].

2.1.2 Rotational velocity

When adding rotational velocity to the system, the rotor and shaft want to expand outwards due to centrifugal forces, which creates a difference in contact pressure for varying speeds. The expression for centrifugal force, F_c, can be seen below

$$F_c = m\omega^2 R \tag{2.3}$$

where ω the rotational velocity, R is the radius and m is the mass.

The new pressure is determined by first calculating the radial displacements, u, of rotor and shaft from the following equations

$$u_r = \frac{(3+\nu_r)(1-\nu_r)}{8E_r} \left(r_{r,i}^2 + r_{r,o}^2 - \frac{1+\nu_r}{3+\nu_r} r_r^2 + \frac{1+\nu_r}{1-\nu_r} \frac{r_{r,i}^2 r_{r,o}^2}{r_r^2} \right) \rho_r \omega^2 r_r \tag{2.4}$$

$$u_s = \frac{(3+\nu_s)(1-\nu_s)}{8E_s} \left(r_{s,i}^2 + r_{s,o}^2 - \frac{1+\nu_s}{3+\nu_s} r_s^2 + \frac{1+\nu_s}{1-\nu_s} \frac{r_{s,i}^2 r_{s,o}^2}{r_s^2} \right) \rho_s \omega^2 r_s \tag{2.5}$$

where ρ is the density and R is the radius where the displacement is calculated [10], [11].

From this, a grip which varies with the rotational velocity can be obtained from

$$\Delta_{rot}(\omega) = \Delta - 2\,(u_r - u_s)\,. \tag{2.6}$$

The contact pressure is determined in the same way as before from equation 2.2.

2.1.3 Torque

The transferable torque M, in a shrink-fit is directly proportional to the contact pressure hence the torque is also dependent on the rotational velocity [12]. The expression for M becomes

$$M = p(\omega) \cdot \frac{1}{2}\mu\pi t d_{o,s}^2. \tag{2.7}$$

The parameter t is the thickness of the laminate and μ is the friction coefficient.

2.2 Analytical contact pressure and torque

The values of the parameters for the analytical solution were chosen to match previously made friction lock tests at Volvo Cars. The base case simulation will also be set up with the same parameters to be able to confirm the accuracy. The calculations and plots are made using Matlab R2019b [13].

2.2.1 Friction lock tests

Previously, friction lock tests have been carried out at Volvo Cars, which were done to determine the friction coefficient between rotor and shaft, which resulted in $\mu \approx 0.1$. The laminate shown in Figure 1.2 together with a shaft with a diameter of 55.5mm were used. During the tests, different grips where tried and the largest one was not possible to assemble. This made it possible to decide what the minimum play had to be during assembling, which is described more in detail in Section 2.3. The torque capacity was also measured during the experiments for a stationary case. These results will be used as a way to verify the accuracy of the simulations.

2.2.2 Results

The curve in Figure 2.2 is calculated by using equations 2.2 and 2.6. It shows how the contact pressure between shaft and rotor decreases with increasing rotational velocity due to the centrifugal force. The contact pressure for the observed geometry drops from the stationary case at $p = 78.24$MPa down to $p = 54.73$MPa at a maximum speed of 16300RPM. The geometry used is given by the parameters in Table 2.1; see Figure 2.1 for reference.

Table 2.1: Parameters used during simulations and calculations for the laminate and the shaft.

	Rotor	Shaft
r_i	27.75mm	20.75mm
r_o	75.0mm	27.75mm
E	163GPa	210GPa
ρ	7.60 g/cm^3	7.85 g/cm^3
ν	0.30	0.30

The nominal grip used during the friction lock tests was $\Delta = 110\mu m$. Hence, the same value is used for the analytical solutions. From equation 2.2 it is obvious that the contact pressure also will decrease linearly with a reduced grip, Δ.

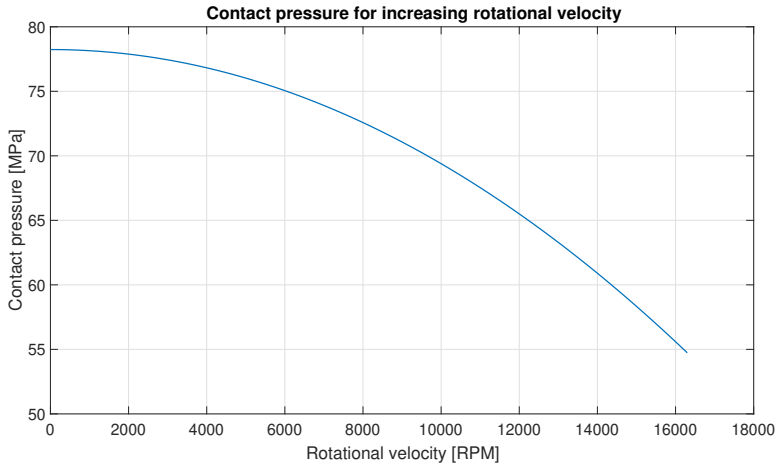

Figure 2.2: Curve showing how the contact pressure decreases with increased rotational velocity with diameter of the shaft $d_{s,o} = 55.5$mm and the diametrical grip $\Delta = 110\mu m$.

The transferable torque as a function of the rotational velocity is plotted in Figure 2.3 by using equation 2.7. The shrink fit's ability to transmit torque is proportional to the contact pressure, which means that the two curves have the same shape. The torque curve is computed by considering one laminate with thickness $t = 0.27$mm and where the friction coefficient is obtained from previous tests and has a constant value of $\mu \approx 0.1$. At 0 and 16300RPM, the transferable torque is 9.65Nm and 6.75Nm, respectively.

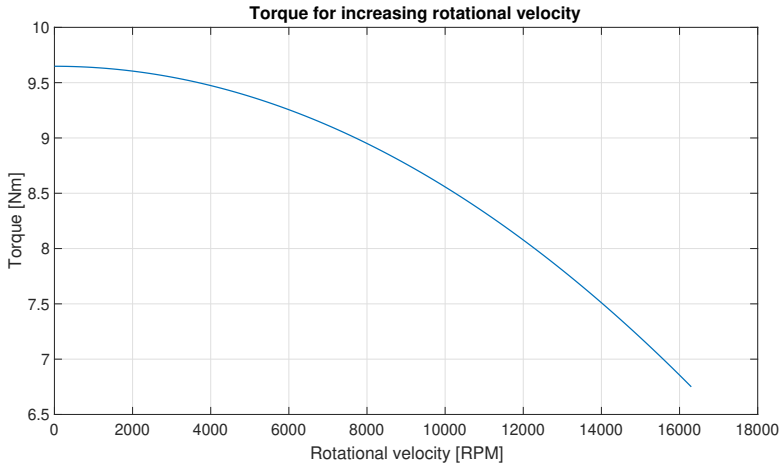

Figure 2.3: Transferable torque for one laminate with a thickness $t = 0.27$mm and friction coefficient $\mu \approx 0.1$.

2.2.3 Torque request

The torque request from the electric machine varies with the velocity. Lower RPMs will have a higher torque request compared to high RPMs. At the highest velocity of 16300RPM, the assembly has to be able to withstand 500Nm. The necessary reaction torque from one laminate is easiest obtained by assuming that the transferable torque is linear with the number of rotor laminates. Hence, the required torque per laminate in a rotor consisting of 440 laminates is 500/440≈1.14Nm. The maximum torque request of 880Nm occurs between 0-5000RPM, which translates to 2.0Nm per laminate. These calculations for torque per laminate are fairly conservative. Therefore the requirements are set to 2.0Nm for the highest RPM and 3.5Nm when maximum torque is requested, which is an increase of 75%.

The torque request includes a shock factor of 1.6. The shock factor ensures that unexpected loads do not break the system. An example of a shock load is when one of the vehicle wheels loses contact with the ground and quickly regains it. The suddenly applied load could turn the shaft relative to the rotor stack, negatively affecting the whole machine's effectivity.

2.2.4 Slip angle

A large slip angle will have a negative impact on the machine's effectiveness, which may occur at high torques and rotational velocities. At this moment, it does not exist a precise value of the slip angle β, which is acceptable, but $\beta > 0.7°$ is considered to be very large. Therefore, it is of great interest to dimension for this. Figure 2.4 shows a schematic image of the slip angle β.

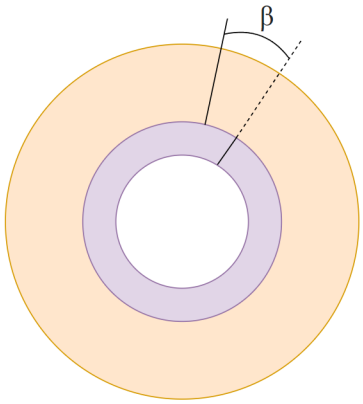

Figure 2.4: Slip angle β between shaft and rotor. A large angle affects the efficiency in a negative way.

2.3 Manufacturing tolerances

Due to manufacturing tolerances, the diametrical grip varies by ±30µm from the nominal one. The shaft's diameter will vary with 10µm, and the center hole of the

laminate with 20µm. Because of this, the assembly process has to be dimensioned for a worst-case scenario, which in this case would be the largest shaft against the smallest laminate. It also has to exist a diametrical play between shaft and rotor for the assembly process. In other words, the size difference between the two parts has to be larger than the grip and play together when cooling the shaft and the heating rotor.

From the previously made friction lock tests at Volvo Cars, the assembly process of rotor and shaft with a shrink-fit failed with a diametrical play smaller than 0.033mm. However, with a diametrical play of 0.035mm, it was possible. To ensure an easy assembly with the worst-case scenario described, a diametrical play of 0.040mm is used.

2.3.1 Possible shrink fit

The maximum possible shrink-fit grip is greatly dependent on the outer diameter, shown in equation 2.1. A larger diameter can shrink and expand more with cooling and heating. The outer shaft diameter was set to $d_{s,o} = 55.5$mm to resemble the real-life tests, as mentioned in Table 2.1.

The rotor laminates are heated to 180°C, and the shaft is cooled to achieve the shrink fit. Instead of cooling the shaft to -150°C using liquid nitrogen, it is assumed to be cooled down to -40°C. With the diametrical play of 0.040mm, and a shaft diameter of 55.5mm, the maximum possible grip to assemble is 105µm. Due to the manufacturing tolerances of ±30µm, the nominal grip must be set to 75µm. The diametrical grip will therefore span between 45µm and 105µm. Figure 2.5 shows how the diametrical play decreases with less cooling of the shaft while the laminate is heated to 180°C. At the shaft temperature of -40°C, the worst case is still possible to assemble.

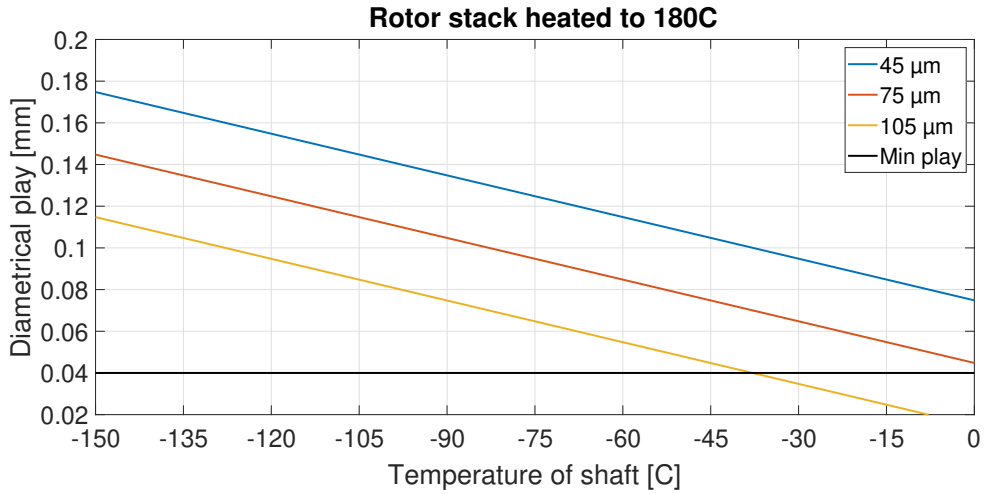

Figure 2.5: Plots of how the diametrical play varies with the the temperature of the shaft. The minimum play to be able to assemble the parts is at least 0.040mm.

A problem arises when the smallest shaft is attached to the largest laminate, namely, when the grip becomes 45µm. The transferable torque at 16300RPM should be at least 2.0Nm which is not fulfilled with this grip, as it only reaches $\approx$ 1.05Nm, see Appendix A.1 for plot over torque with $\Delta = 45$µm. Since the shrink fit cannot transfer as much torque as requested, alternative geometries of the cross section are investigated to find a solution to this problem.

3

Base Case

A base case of the simplified geometry and shrink fit used at Volvo Cars today is created in ANSA and simulated in Abaqus to have a model to compare other geometries with. The discussion about mesh quality and element type will be the same also for the alternative geometries. The basis for the model comes from the friction lock tests. Together with the tests and analytical solutions, the simulations are verified.

3.1 Simplified models

The alternative cross section geometries are simplified to increase modeling speed and reduce simulation time. The base case is made in the same manner to have a good comparison between the results from the models. When stresses and pressure are analyzed for the base case, only 1/16 of the whole cross section is observed as it simplifies the model even further. This simplification is possible since the two parts are axisymmetric, making it possible to use a smaller mesh area, hence a shorter computational time. Figure 3.2 shows how the geometry is modeled when contact pressure and von Mises stresses are examined. When torque and slip angle were analyzed, the whole shaft and laminate were required to be used. The torque, which comes from the friction force, depends on the area in contact. If not the complete area was used, the transferable torque would have become lower.

3.2 Mesh theory

All meshes are created with second-order elements. Second-order elements can mimic the real geometry better than first-order elements, and they increase the calculations accuracy and resemble the real world better when applying loads and displacements [14]. Figure 3.1 shows how a piece-wise linear function (left) is approximated using **one** first-order linear element (middle) versus using **one** second-order quadratic element (right) [14]. Obviously, the higher-order mesh will capture the actual geometry and deformations better than the first-order mesh. Grey area is shows the error.

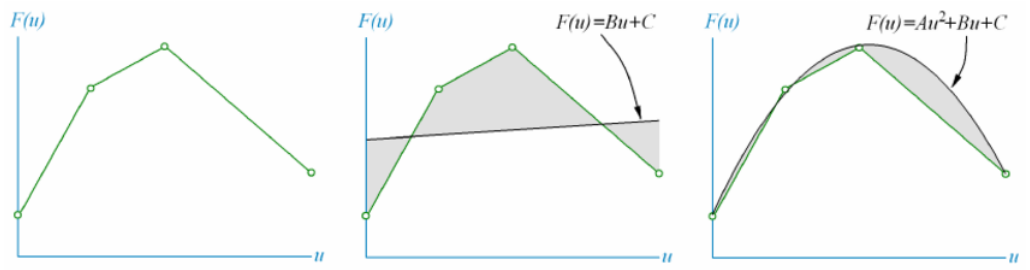

Figure 3.1: First- versus second-order elements approximation of a piece wise linear function, image from Benjamin F. Gregorskis paper: Contouring Curved Quadratic Elements [14].

Elements along the outer edge of the laminate were made larger than the ones close to the inner diameter to decrease the number of elements of the mesh and thereby reduce the computational time. The area of interest is where the shrink fit happens and not in the rest of the laminate, hence the reduced resolution of the mesh can be adopted elsewhere. Figure 3.2 illustrates the mesh used for the base case simulations.

3.2.1 Contact elements

The contact between the shaft and the laminate was defined as a general contact in Abaqus, where a surface-to-surface contact formulation was used [15]. The laminate is more likely to be deformed than the shaft due to lower Young's modulus and larger centrifugal forces acting on it. Hence a more precise mesh was created with smaller elements along the inner edge to capture its deformation more accurately. The general contact should be defined using one slave and one master surface, where the master surface is stiffer and have a coarser mesh [15]. Therefore the outer boundary shaft with a lower resolution of the mesh was chosen as the master surface and the inner boundary of the laminate as the slave surface.

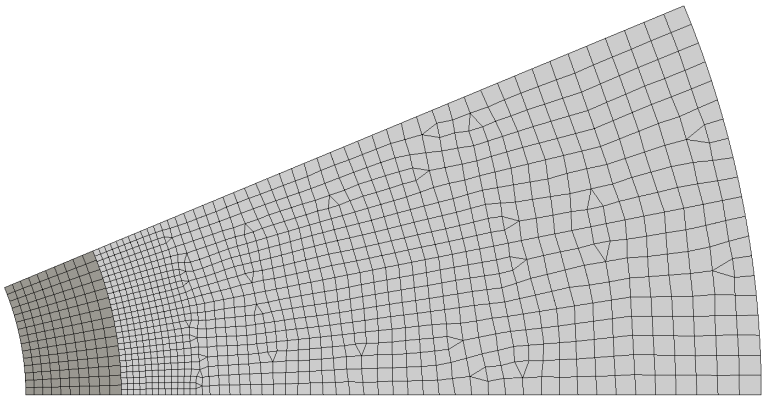

Figure 3.2: Mesh of 1/16 of shaft and laminate using second order elements. The elements on the laminate closest to the shaft are made smaller to capture what is happening accurately.

3.3 Model set up

The geometry was modeled in ANSA with linear elastic materials and part properties selected as in Table 2.1. Since one laminate only has the thickness of $t = 0.27$mm the model is created in 2D. The elements are of the type `CPS`, which implies that a plane stress case is assumed [15]. Due to the circular shape of the laminate and shaft, the mesh was transformed in to polar coordinates to facilitate the definition of loads and boundary conditions.

The simulation is divided in to three different time steps:

- **Step 1:** Shrink fit
- **Step 2:** Centrifugal force
- **Step 3:** Torque

Step 1 simulates the shrink fit. In Step 2, the rotational velocity is simulated by applying a centrifugal load onto all elements of the mesh, and step 3 is where the laminate is rotated around the shaft (which is fixated) to measure transferable torque and slip angle.

3.3.1 Interference

The interference between laminate and shaft was modeled using a `CONTACT INITIALIZATION DATA` (CID) together with `CONTACT INITIALIZATION ASSIGNMENT` (CIA) [15]. The shaft and laminate were created with $r_{r,i} = r_{s,o}$, thus without any interference, but with the CID it is possible to define the radial grip with ease. The CIA was used to choose which surface to be master and slave for the interference, and as discussed in section 3.2.1, the shaft was selected as master and laminate as the slave surface. This causes the elements at the inner edge of the laminate to stretch out, overlapping the elements on the shaft. The two parts are then pressed away from each other by the overlapping, creating the contact pressure which fixates them together [15]. A constraint that occurs due to the stretching of the elements from the laminate is their size. To not get elements of bad quality, which here would be an aspect ratio larger than three, the elements had to meet the requirement from the equation 3.1 below, see also Figure 3.3, here shown for a rectangular element.

$$\frac{L + \Delta}{W} < 3 \tag{3.1}$$

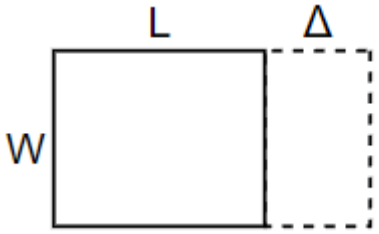

Figure 3.3: An element stretched out the length of the grip Δ. The width and length of the element is labeled W and L.

For non-rectangular elements, the longest side is divided by the shortest side in equation 3.1.

3.3.2 Loads and boundary conditions

To hold the shaft and laminate in place, the nodes at the inner edge of the shaft are locked in the tangential direction, restricting rotational movement. The nodes at the outer edge of the laminate is connected to a node in the center of the system via a `COUPLING` [15], shown in Figure 3.4. The center node is then able to control all the connected nodes. During time steps 1 and 2, the center node is locked rotationally around the z-axis, but in step 3, a prescribed rotation is applied to the center node, which rotates the laminate around the fixated shaft. By doing this, it is possible to measure the torque capacity and slip angle.

To mimic the rotational velocities which the system are subjected to, a centrifugal force is applied to all elements in the radial direction. The force per volume is dependent on the radius. Hence, the force increase with the radius, see equation 2.3 [15].

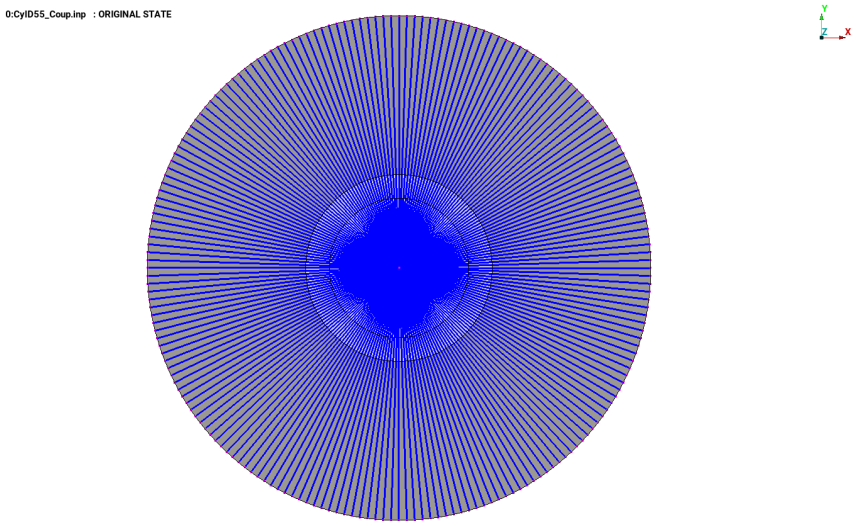

Figure 3.4: The coupling is connecting the outer edge of the laminate to a node in the center of the system. The node is turned around the z-axis and torque as well as slip angle are measured.

3.4 Base case analysis

After the base case had been simulated with the parameters shown in Table 2.1 and with thickness $t = 0.27$mm and grip $\Delta = 110$µm contact pressure and torque capacity results were produced using META. These results were then compared to the analytical solution to ensure accuracy of the simulations. Figure 3.5 and Appendix A.2 illustrate the contact pressure by only observing the elements in contact at 16300RPM and no rotational velocity, respectively. The pressure for the

two velocities is equal to 54.79MPa and 78.35MPa. Compared to the analytical values mentioned in Section 2.2, the difference is less than 0.15%. This small error indicated that the modeled shrink-fit method was working as intended.

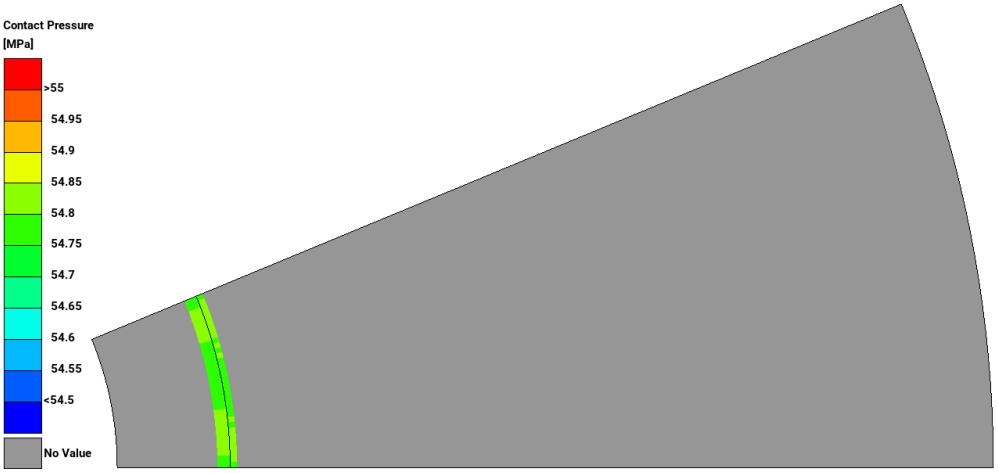

Figure 3.5: Contact pressure at 16300RPM with diametrical grip $\Delta = 110\mu m$.

In Figure 3.6, the transferable torque at 16300RPM for the base case can be seen. The two first seconds in the plot are time steps 1 and 2, where turning of the laminate begins after 2 seconds in time step 3. The torque capacity was measured by observing how much moment the center node could withstand before the rotor was released from the shaft. The maximum torque was measured at 6.75Nm, a difference of 0.05% compared to the analytical solution. Hence, the method of measuring transferable torque is sufficient.

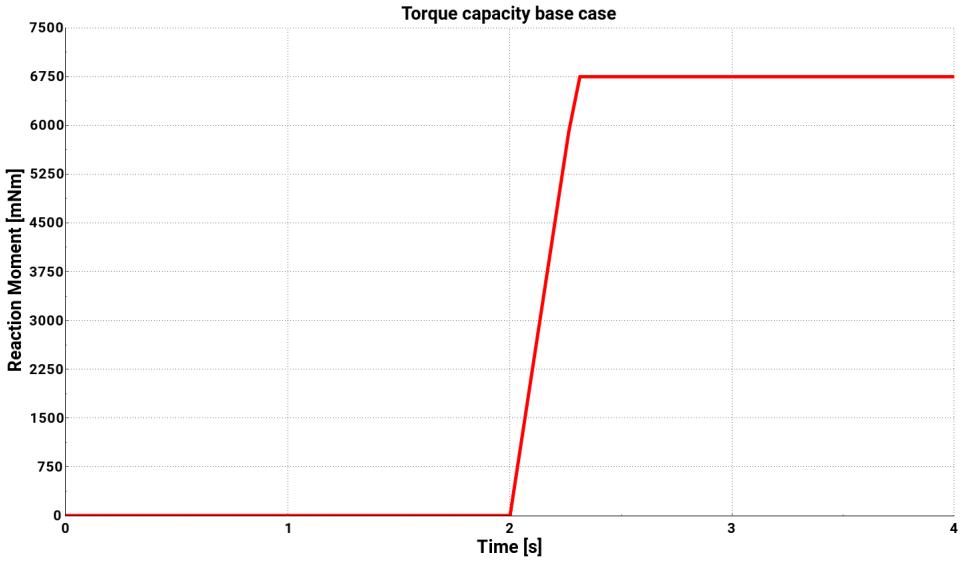

Figure 3.6: Transferable torque at 16300RPM with diametrical grip $\Delta = 110\mu m$.

3.4.1 Smallest grip

From the analytical solution, a grip of 45µm was not sufficient to transfer enough torque at 16300RPM, which motivates the need to investigate alternative geometries. The simulation confirms this further as the torque capacity seen in Appendix A.3, is equal to 1.05Nm when the laminate lets go of the shaft, which again, is below the required 2.0Nm.

3.5 Slippage

The slip angle β for the base case is shown in Figure 3.7, measured in degrees. It is measured by observing the angle between two points, one point on the fixated shaft and one on the inner edge of the laminate while the outer edge is turned (same method as for measuring torque). From the simulation, the slip angle became $\beta = 0.00205°$, which is way below the maximum criteria of 0.7°. The slip angle for the base case geometry is never in danger of crossing the largest allowable value. Instead the problem with this fixation is the torque capacity mentioned in Section 3.4.1 above.

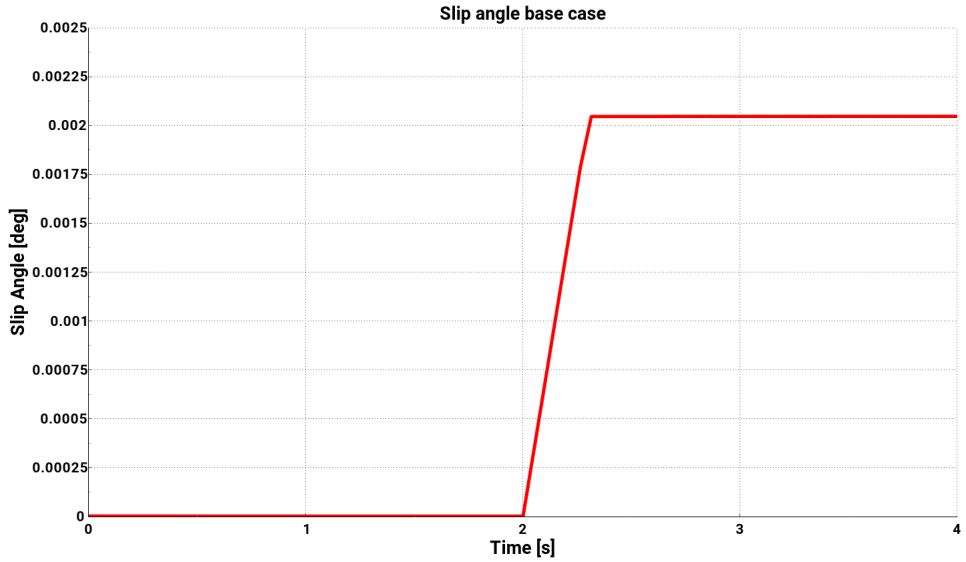

Figure 3.7: Slip angle at 16300RPM with diametrical grip $\Delta = 110$µm.

3.6 Stresses

Stress analyses are performed for the two parts to locate any stress concentrations. Figure 3.8 shows how the signed von Mises stress (defined in Section 3.6.1 behaves throughout the shaft and laminate at 16300RPM. Due to the simple circular geometry, no stress concentrations appear. Similar results were shown at zero and 5000RPM, where the stress remains even across the two parts, see Appendix A.4 and A.5. The higher stress at the laminate's inner edge is due to the outwards pressure from the shaft. Whereas the highest stress for the shaft is located at the

inner edge. This is because a smaller radius means a smaller area, which in turns gives a larger stress.

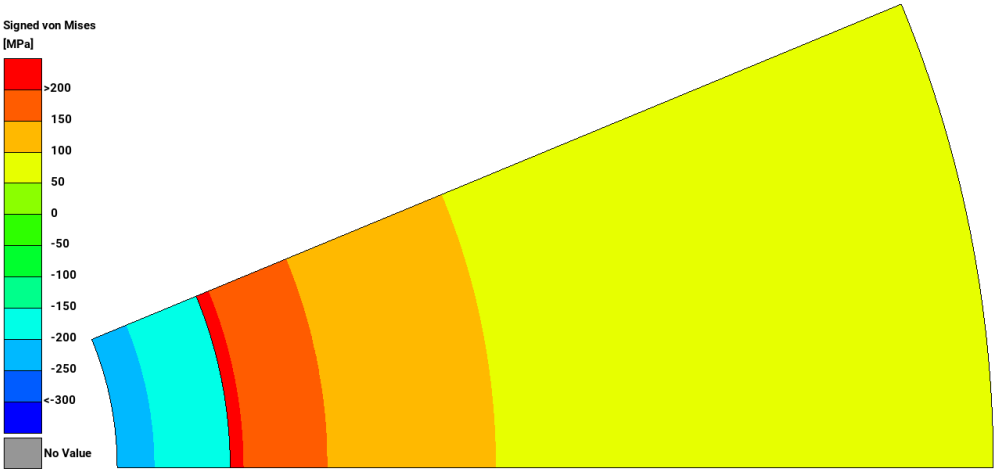

Figure 3.8: Signed von Mises at 16300RPM with diametrical grip $\Delta = 110\mu m$.

3.6.1 Signed von Mises

Regular von Mises stress always has a positive value, but in Abaqus there exists a measurement called signed von Mises stress which also considers if the stresses are compressive or tensile. The sign is taken as the sign of the hydrostatic stress , while the magnitude is the normal von Mises stress [15]. It is of great interest to know if the stresses come from the centrifugal force's tensile load or the compressive load from the interference fit since it contributes to a better understanding of why the material behaves in a certain way.

4
Alternative Geometries

To be able to meet the requirements with decreased grip, new geometries for the cross section is investigated. The geometries are tested against transferable torque and slip angle while trying to keep high manufacturability. Finally, the shape which fulfills the requirements most efficiently is chosen to be further optimized.

4.1 Tested geometries

All tested geometries originated from and were compared to the circular shaft with a diameter of 55.5mm. To create the different geometries, material was removed from the original shaft. The inner edge of the laminate was then matched with the new geometry of the shaft. The expansion and contraction of the laminate and the shaft during heating and cooling greatly depends on the diameter, therefore the smallest generated diameter is set as the limit for the possible grip, see Figure 5.7 for grip as a function of diameter.

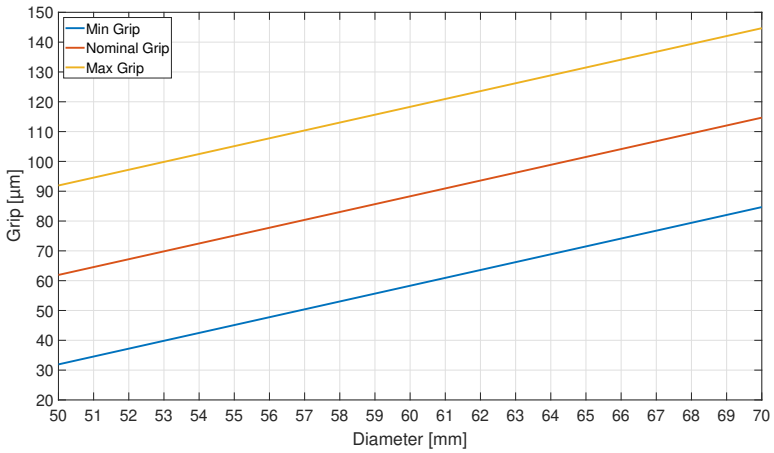

Figure 4.1: Possible grips for different shaft diameters. Larger diameter makes it possible to use a bigger grip.

The creation of the alternative geometries was done by trying out different geometrical functions, such as ellipse, super ellipse and trigonometric curves. The different functions made it possible to test curvatures and amplitudes easily. Also, geometries adjusted for grinding tools creating the shapes were tried out, as these would have

high manufacturability.

The geometries are created regarding the ability to be manufactured, limiting the possibility of creating certain shapes. The shaft will constrain the possible shapes due to the manufacturability. The new shaft geometries are shaped by a grinding processes, gradually removing material from a circular shaft. With less material to remove, the easier and faster the shaft could be created. Since the laminates are punched or laser cut from sheet metal, the possibility of creating more intricate shapes is no problem.

The model is set up in the same way as the base case model; loads, boundary conditions and shrink fit are all applied in the same manner. The mesh resolution was also of the same quality. Torque capacity and slip angle are extracted similarly but instead, plotted against each other. The reason for this is to be able to observe the slip angle at the requested torque. Some of the geometries does not loose contact between shaft and laminate, and instead greatly deforms and at the same time, transferring excessive amount of torque.

4.1.1 Ellipse

The first tested geometry was the ellipse which has the mathematical formula seen in equation 4.1, where a and b are the two radii. [16].

$$\frac{x^2}{a^2} + \frac{y^2}{b^2} = 1 \tag{4.1}$$

This shape has only smooth edges but a varying curvature. The maximum allowable grip with this geometry is calculated from the smallest radius since it limits the expansion and contraction of the two parts.

4.1.2 Superellipse

The mathematical formula for the generalized superellipse is [17]

$$\left|\frac{x}{a}\right|^n + \left|\frac{y}{b}\right|^n = 1 \tag{4.2}$$

where n is a positive number. By increasing the value of n, the shape goes from a rhombus shape to a rectangle with rounded corners. Simulations of geometries created with $n > 1$ were carried out and compared. When $n = 4$ and $a = b$, the shape is called squircle[18]. In Figure 4.2 the outer edge of the shaft has the shape of a squircle.

The geometry does not have any sharp corners, but due to its shape it has the ability to mechanically transfer torque without friction.

Figure 4.2: Geometry of super ellipse when $n = 4$ and $a = b$. The specific shape is called squircle.

4.1.3 Flower shape

By using a cosine function, a geometry that will be called the flower was created. It was done by plotting the cosine function in a polar coordinate system,

$$r(\theta) = R + A\cos(\theta n) \tag{4.3}$$

where R is the outer radius of the shaft and A is the amplitude. Here, θ range over one revolution, making it possible to choose the frequency with n. Figure 4.3 shows the geometry with $n = 8$, namely eight periods.

Figure 4.3: Image of the Flower shape. The Geometry are created from a cosine wave plotted in a polar coordinate system.

The name originates from the fact that the shape resembles a flower. This shape is similar to a key- or spline joint, but without large curvature changes which removes sharp edges and minimizes the problem with the tangential expansion of the keys,

in this case, the peaks of the cosine function.

The creation of the shape is restricted to the size of the grinding tool, where a smaller diameter of the tool makes it possible to create deeper cuts and more periods. In Appendix A.6 a graph of what amplitudes and number of periods which are possible to manufacture with a grinding tool with a diameter of 50mm.

4.1.4 Valleys

One geometry that emerged from the cosine function is here called Valleys. The shape is similar to the flower but without peaks, and the valleys have a circular shape instead of a cosine wave. Because the grinding tool also is circular the manufacturability with this geometry is higher than for the flower. Figure 4.4 illustrates what the geometry looks like.

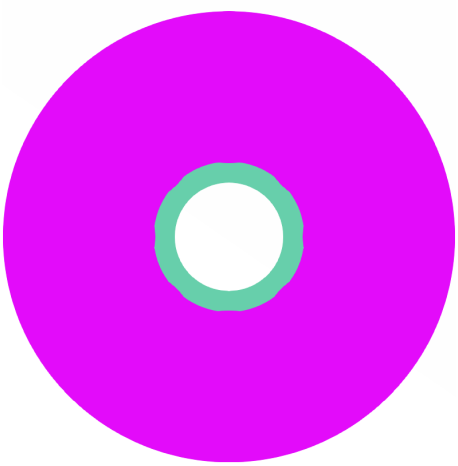

Figure 4.4: Image of the Valley shape. The valleys are created from the shape of a piece of a circle.

At the beginning and end of each valley a corner will emerge. A deeper valley will generate a sharper corner angle, creating higher stress concentrations, see Appendix A.7 for close up of sharp corner. The advantage of the sharper angle is that the transferable torque increases and slip angle decreases.

4.2 Geometry analysis

The requirements that were considered when selecting the geometry were transferable torque and slip angle. In Figure 4.5, results from four alternative geometries and the base case are plotted. The plot shows slip angle versus transferable torque at 16300RPM, where a torque of 2.0Nm is wanted. The same models are also plotted at 5000RPM in Appendix A.8, here the sought after torque is 3.5Nm. All the tested geometries manage to withstand the torque at 5000RPM. The parameters for the plotted geometries can be seen in Table 4.1, where the grip is chosen with

the geometry's smallest diameter and worst case with respect to tolerances from the plot in Figure 5.7.

Table 4.1: Parameters used to create the models for which the results are plotted in Figure 4.5

	Diameter [mm]	Grip [µm]	Amplitude [mm]	No. of periods
Circle	$2R = 55.5$	45	-	-
Ellipse	$2a = 55.5, 2b = 53.5$	40	-	-
Squircle	$2a = 2b = 46.7$	30	-	-
Flower	2R=54.5	44	0.25	16
Valleys	2R=55.0	45	0.25	16

The plotted models was chosen as they showed interesting results or greater performance. Geometries with other parameters did not show the same striking results or an outcome worth noting.

4.2.1 Torque

As seen in Figure 4.5, three out of five geometries managed the torque request, squircle, flower and valleys. This is believed to be because that a more rapid change in radius is better than a larger but smoother change to achieve the torque request. Why the ellipse performers worse than the base case circle is most likely because a smaller grip needs to be used, which does not compensate for the new geometry. The reason for the valleys being better than the flower is probably due to the steeper valleys.

4.2.2 Slip angle

The slip angle is the relative angle between the shaft and laminate and is explained in Section 2.2.4. Again, in Figure 4.5 it can be seen that the circle and the ellipse shape are not capable of handle the required torque of 2.0Nm. The squircle can withstand the torque, but the slip angle is much larger compared to the flower and valleys. The reason for the large slip angle for the squircle is that the laminate loses contact with the shaft due to the centrifugal forces because of the small grip.

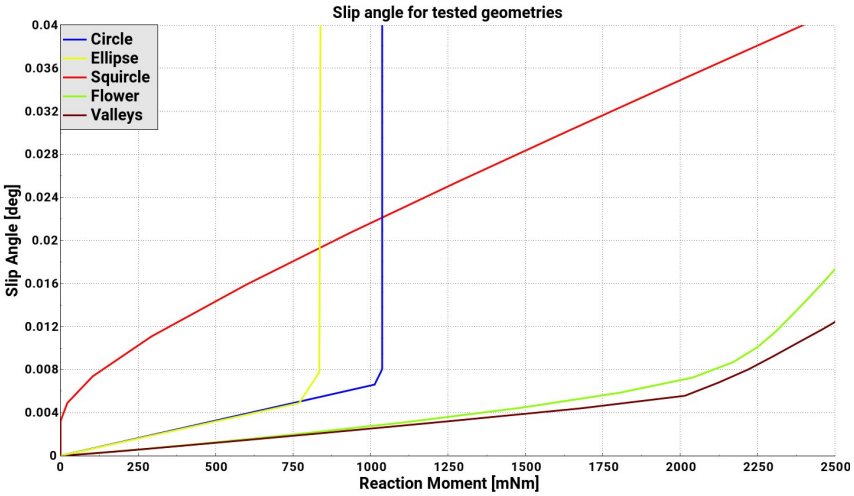

Figure 4.5: Plot of slip angle versus reaction moment at 16300RPM for the different geometries.

4.3 Selected geometry

From the presented results, the geometry chosen to be optimized is the valleys. This is because this geometry had the best performance regarding transferable torque and slip angle. Since the valleys on the shaft would match a grinding tool, the ability to manufacture it is also better than the flower geometry. The valley geometry requires less material to be removed from the shaft compared to the other geometries.

5

Optimization

The valley shape is chosen for further development. This chapter will describe the optimization process, which is done by considering various diameters and valley geometries using the real laminate and including the magnets. The solution will be optimized against slip angle and von Mises stress.

5.1 Simulation set up

The same material parameters, boundary conditions and load set up as those used in the simplified cases were also used for the valley optimization process. The difference is the new laminate, the contact definition for the magnets, a higher mesh resolution to capture the more intricate geometry and a script for creating new geometries.

5.1.1 Real laminate

Figure 5.1 shows a real laminate with magnets, similar to the one used in the simulations (due to confidentiality the actual one can not be shown). The transferable torque with the real laminate is lower than for a solid disc. The laminate in Figure 5.1 has eight lightening holes to make the assembly lighter, but in turns, lowers the strength resulting on the reduced torque capacity. The material between the lightening holes are called bridges. When comparing results from the friction lock tests with the simulation without rotation speed, the difference in transferable torque was only 2.5%. This implies that the simulation is modeled in a way that resembles the reality, in Appendix A.9 the torque capacity is plotted from the simulation showing 7.46Nm, which is the maximum torque. It does not exist any real life testing to confirm the simulations for torque capacity at high velocities, therefore the results are purely theoretical.

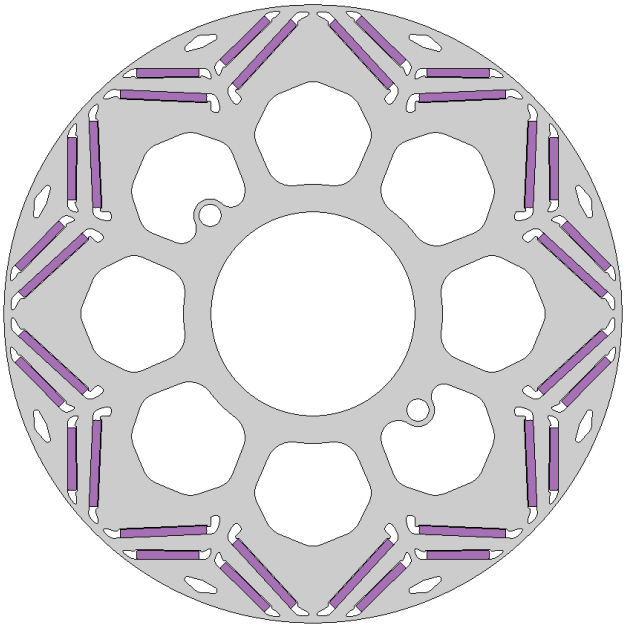

Figure 5.1: Real laminate with magnets, similar to the one used in simulations and friction lock tests.

5.1.2 Magnets

The simulations are set up in the same as before, but now with magnets. The simulations had trouble converging if the magnets were defined with a general contact between shaft and laminate. Instead, the magnets are connected to the laminate using a `TIE`. This fixates the magnets to the laminate, preventing them from small movements, making the model robust and simulations more likely to converge. Figure 5.2 shows the difference between tied and general contact with the applied centrifugal force at 16300RPM.

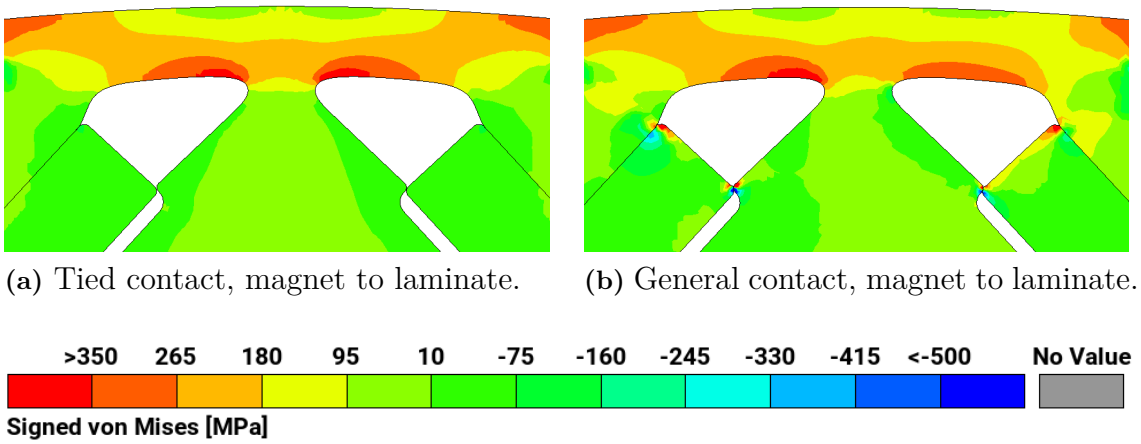

(a) Tied contact, magnet to laminate.

(b) General contact, magnet to laminate.

Figure 5.2: Comparison of tied contact and general contact with same scales. General contact makes it difficult for simulation to converge.

When using a general contact (5.2b), stress concentrations occur at the corners of the magnets and on the nearby edges of the laminate. The magnets modeled with the tied connection (5.2a) does not appear to have any increased stress in the same areas. However, the stresses in the rest of the laminate are relatively unaffected by the choice of modeling. Hence the chosen way to model the contact for the magnets is therefore with a tied contact. The area of interest in the analysis is also where the shrink fit happens and not in other parts of the laminate.

5.1.3 Parameters of optimization

The valley geometry will be altered with the parameters: amplitude of valley (A), number of valleys (N), and shaft diameter (D). The amplitude describes the valley's depth which is how deep the grinding tool will go into the shaft. Table 5.1 below lists the range and quantity of the tested parameters values.

Table 5.1: Parameters used to optimize the geometry for the given requests.

Parameter	**Range**	**Quantity**
Amplitude	0.10-0.35 [mm]	6
No. of valleys	2-30 [-]	14
Diameter	50-70 [mm]	4

Figure 5.3 shows an exaggerated example of a geometry to display how the parameters affect the cross section more clearly. The geometry is created with $A = 1$mm, $D = 55.5$mm and $N = 8$, where the amplitude's value is much larger than the simulated ones. The small cutouts seen in the laminate is described in Section 5.1.4. Appendix A.10 and A.11 show the laminate and shaft separated.

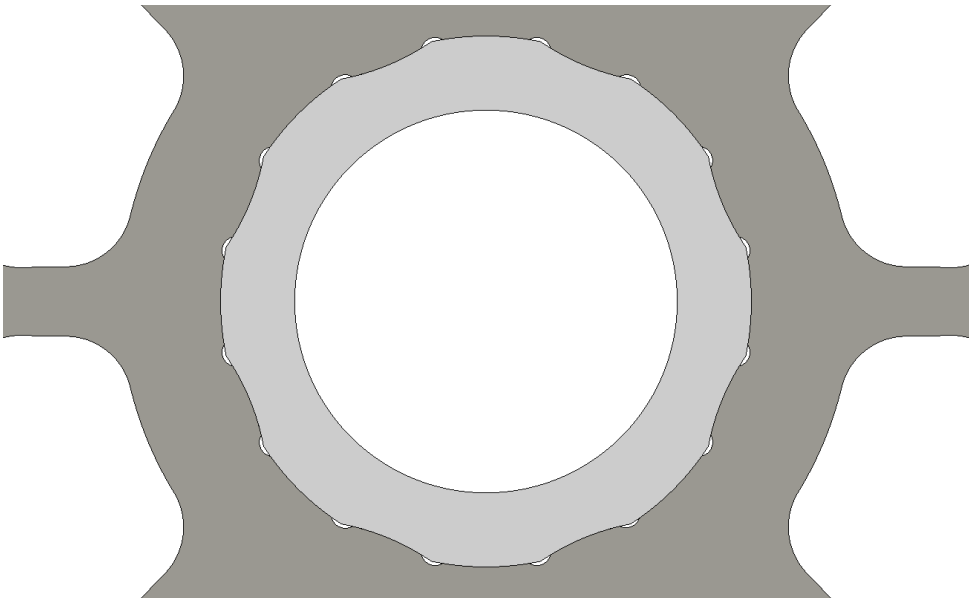

Figure 5.3: Laminate and shaft with adjusted geometry. The image is exaggerated to better illustrate how the parameters affect the shape.

5.1.4 Laminate cutouts

To reduce stress in the laminate, cutouts were made at the edges of the valleys since that is where stress concentrations occur. The cutout geometries are made by drawing two circles. The first circle is drawn at the valley's edge and defines the cutout length. The second circle intersects the first circle and defines the cutout depth, see Figure 5.4. Five different cutout geometries were tested for a model with N=8, D=55.5mm and A=0.25mm.

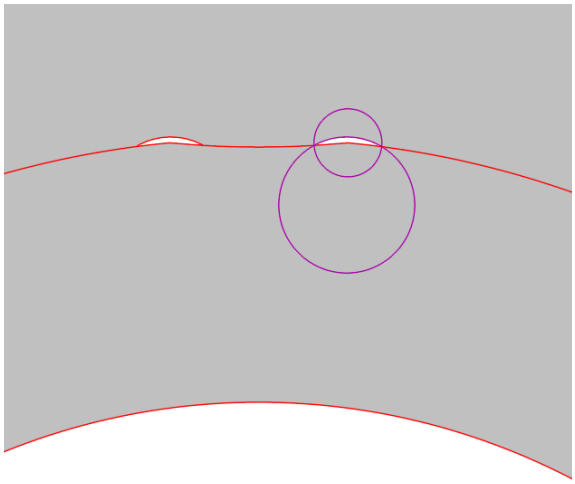

Figure 5.4: Image of the laminate cutouts. The purple circles defines the length and the radius of the cutout.

The tested cutouts had a varying length between 0.3mm and 1.3mm with a radius set to give a depth of 0.1mm. Appendix A.12 shows a close up of the sharp corner and cutout made in the laminate.

5.1.5 Geometry script

To make the optimization process more efficient a python script was created and used to increase the modeling speed. The script asks the user for input on diameter, amplitude and the number of valleys. The valleys are then cut out from the shaft and changed to be part of the laminate instead. The script is found in Appendix B.1.

5.2 Results

The joint's requirements which are considered are torque, slip angle and stress. It must be able to handle a torque of 2.0Nm per laminate including the shock torque described in Section 2.2. The tests are done on both the smallest, nominal and largest grips, but the smallest grip always results in the highest stress and slip angle. The reason is that a larger shear stress acts on the valleys when the friction is lower. When testing all variants of the valley geometries the torque target was fulfilled. The simulations are carried out with the minimum grip from Table 5.1.

Both laminate with and without the cutouts were tested with the varying parameters as described in section 5.1.3.

5.2.1 Base case

A base case study was also done for the real laminate. This is done to compare the slip angle and the stress distribution to the new geometries. The base case has a circular interference region between shaft and laminate as shown in Figure 5.1. The resulting slip angle is 0.0044 degrees seen from the plot in Figure 5.5. From the plot, it is also possible to see that the maximum transferable torque is around 2.6Nm.

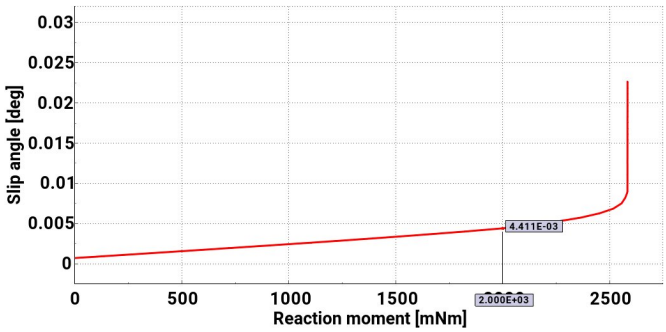

Figure 5.5: Plot of the slip angle vs torque the base case with a grip of 110µm

The stress distribution close to the interference area between shaft and laminate is shown in Figure 5.6. The stress is measured as signed von Mises, described in section 3.6.1. The largest stresses in the laminate are located in line with the bridges. This is where the laminate expands the least. Having more material close to the shaft gives a smaller deformation from the centrifugal force resulting in a higher contact pressure. The whole laminate can not be shown due to confidentiality.

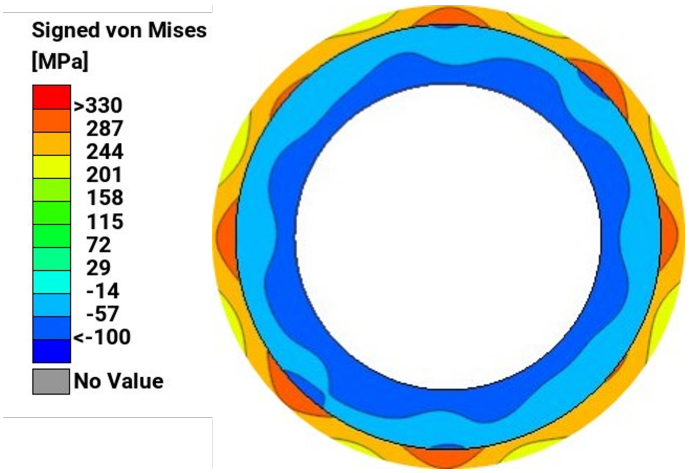

Figure 5.6: Plot of the stress distribution close to the interference area using the real laminate.

5.2.2 Amplitude and shaft diameter

The amplitude and shaft diameter's effect on the slip angle is tested with 16 valleys. With a larger shaft diameter, a greater grip can be achieved because the laminate will expand more when heated up, as discussed in Section 2.3.1. The possible grip for different shaft diameters are seen in Figure 5.7. The weight of the whole assembly also gets lighter with a larger diameter.

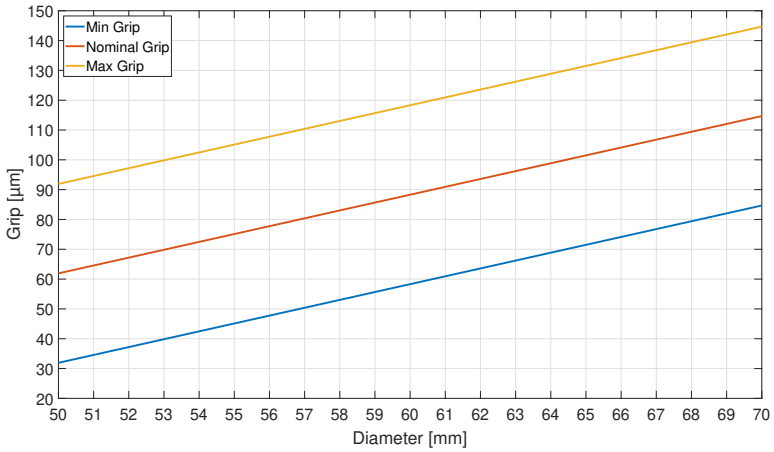

Figure 5.7: Possible grips for different shaft diameters. Larger diameter creates the possibility to use a bigger grip.

Four different shaft diameters are tested with the lowest grip stated in Table 5.2.

Table 5.2: Lowest, nominal and highest grip for the tested shaft diameter. The grip varies with ±30µm due to manufacturing tolerances.

Shaft diameter [mm]	Minimum [µm]	Nominal [µm]	Maximal [µm]
50	32	62	92
55	45	75	105
60	58	88	118
70	85	115	145

A diameter around 55mm seems to be the optimal when considering the slip angle. At a diameter of 70mm the slip angle becomes much larger. The reason for this is due to the decreased distance to the lightening holes, resulting in a decreased ability to withstand the centrifugal force. The results can be seen in Figure 5.8.

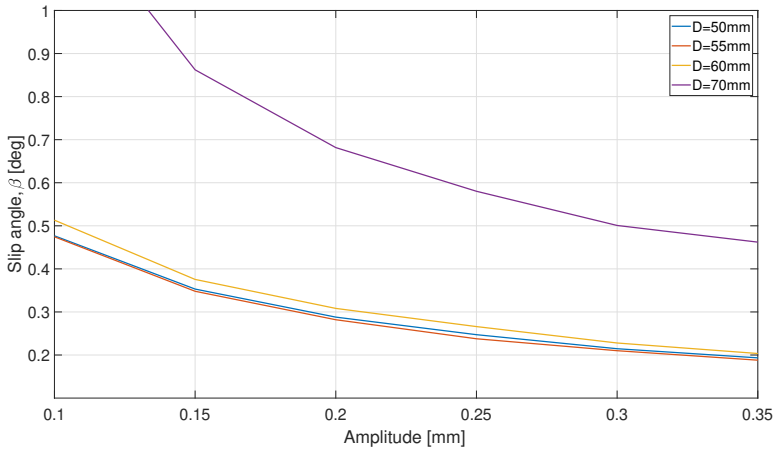

Figure 5.8: Plot of slip angle for different amplitudes and shaft diameters.

With a higher amplitude the slip angle becomes smaller because of the larger contact area and sharper corners at the valley edges making it more similar to a key joint.

5.2.3 Number of valleys

The number of valleys was examined with the constant parameters of A=0.25mm, D=55.5mm. Figure 5.9 shows that the slip angle will decrease with an increasing amount of valleys. The reason is the increasing contact area, resulting in smaller deformations of the valleys. The slip angle halves when the number of valleys doubles because the contact area doubles. The smallest possible angle when varying the number of valleys at 16300RPM is 0.12°. When applying the smallest grip the laminate loses contact with the shaft, therefore the laminate has to be turned 0.12° before contact. When applying the nominal grip the laminate and shaft remain in contact at all velocities and therefore the slip is always lower, which can be seen in Figure 5.9 below.

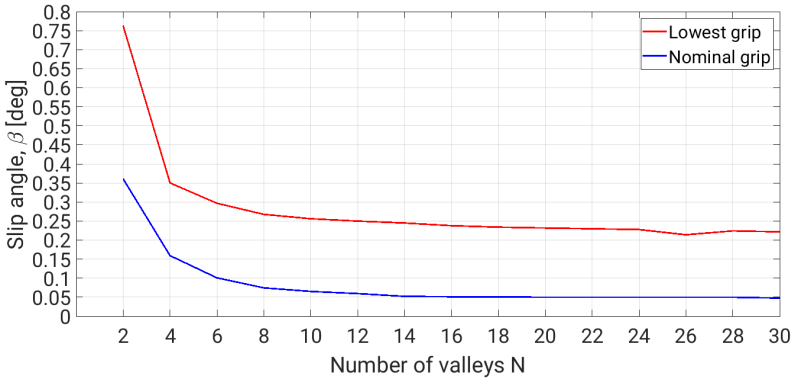

Figure 5.9: Plot of slip angle for different amounts of valleys. Minimum grip is the red curve and nominal grip is the blue curve.

The positions of the valleys has an impact on the slip angle. The reason for this is that the contact pressure will vary around the shaft. For maximum contact pressure

at high RPM the valleys should be placed in line with the lightening holes. This is because the centrifugal force acting on the material outside of the lightening holes will pull the bridges outwards, creating a larger expansion.

However, at stationary case or low RPM the valleys should be placed in line with the bridges due to more material contracting onto the shaft, creating a larger contact pressure. In Figure 5.10 shows where the contact pressure is highest for stationary and maximum velocity.

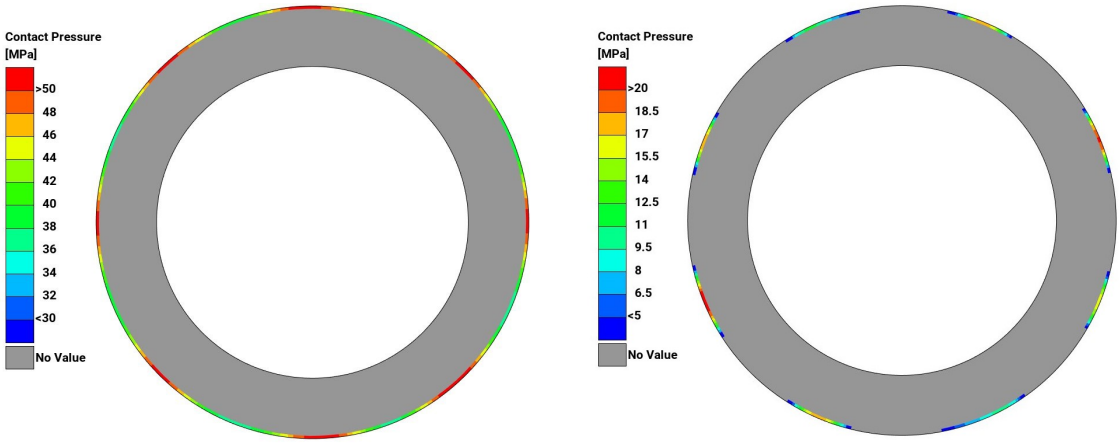

(a) Only shrink fit. **(b)** Shrink fit and centrifugal force.

Figure 5.10: Plot of a circular shaft showing the contact pressure from the real laminate using only a shrink fit and also a shrink fit with centrifugal force applied. The bridges are located at the highest pressure areas in 5.10a

When the grip is lower the laminate loses contact everywhere at the highest RPMs and therefore the position is irrelevant. Instead A comparison at 5000RPM is done. Figure 5.11 shows the comparison where the valleys are placed in line with the bridges (blue) and in line with the lightening holes (red). This is done at 5000RPM since it is the velocity with the largest torque request.

Figure 5.11: Comparison between valleys positioned in line with bridges and in line with lightening holes at 5000RPM.

To make sure that the number of valleys effect on slip angle is independent of the amplitude, 12 and 16 valleys were tested against each other with varying amplitude. The results in Figure 5.12 show that the difference between the two graphs is constant, which means that number of valleys and the amplitude effect the slip angle independently.

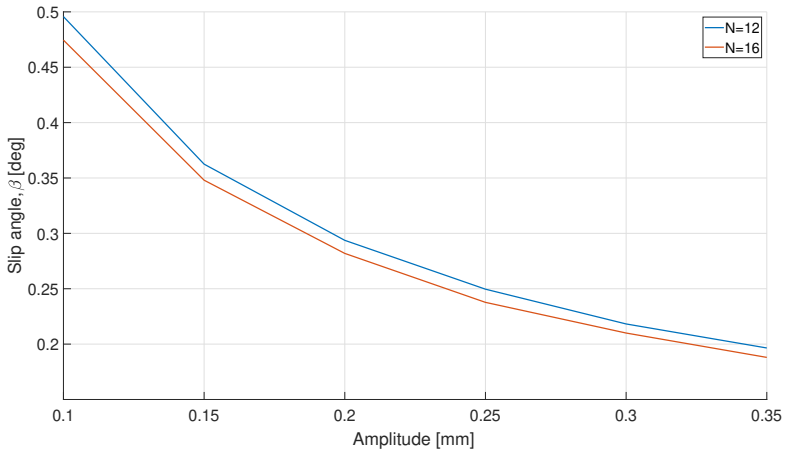

Figure 5.12: Plot of slip angle with increasing amplitude for geometries with 12 and 16 valleys.

5.2.4 Stress analysis

The largest stress occurs in the laminate at the edge of the valley when it hits the shaft in the rotation step of the simulation. This stress varies depending on the number and amplitude of the valleys. With more valleys the stress decreases because the shear stresses acting on the valleys are distributed on more valleys. The lowest stress is found for 24 valleys. The results for the nominal and smallest grip can be seen in Figure 5.13.

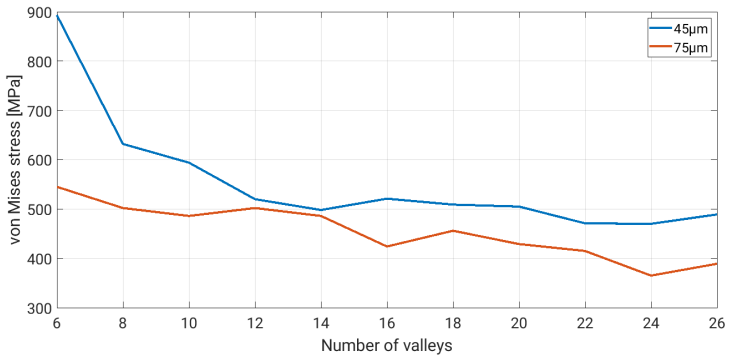

Figure 5.13: Maximum von Mises stress in the valley for different numbers of valleys.

If the amplitude is changed, the stress seems to first increase but with amplitudes deeper than 0.15mm, the stresses decreases. In Figure 5.14 varying amplitude can

be seen for different shaft diameters.

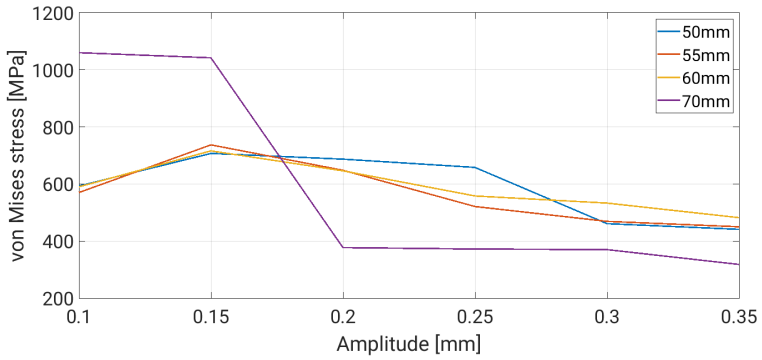

Figure 5.14: Plot of the maximum von Mises stress in the valley with varying amplitude

The effective stress for all geometries are close to the yield limit for the laminate which is 421MPa.

5.2.5 Laminate cutouts

A smaller cutout length resulted in a smaller slip angle because the valleys' edge got closer to the edge of the cutout. The results are seen in Figure 5.15. The stress also varies with different cutout lengths.

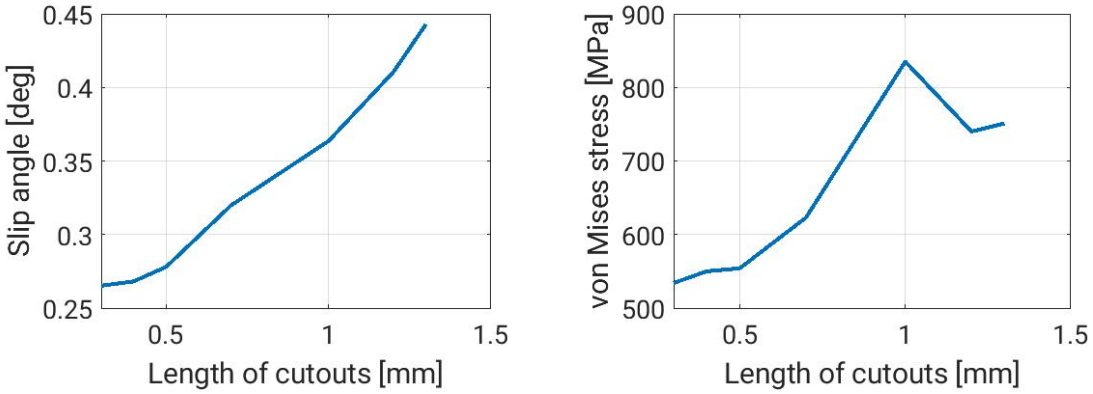

(a) Slip angle **(b)** Maximum stress

Figure 5.15: Slip angle and stress varies for different geometries of the cutouts.

When the cutouts were introduced the stresses decreased for all variants. A plot comparing the geometries with cutouts and without cutouts for different amount of valleys can be seen in Figure 5.16. Here the cutout length is set to 0.6mm. The cutout depth was also tested, but it had no significant effect on the stress or slip angle.

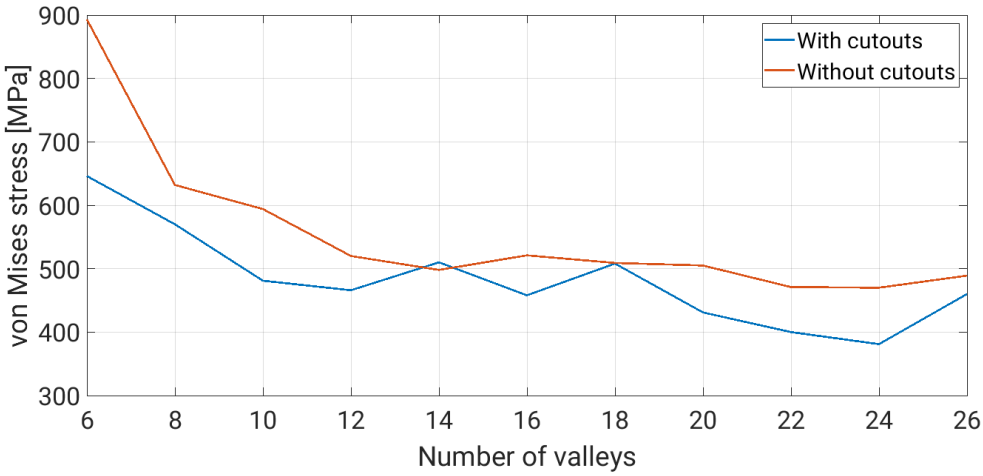

Figure 5.16: Plot of the maximum von Mises stress in the valleys with and without the cutouts.

6
Conclusion

The final design has 24 valleys placed with 8 of them aligned with the bridges. The reason for choosing 24 valleys is that it gives the lowest stress seen in Figure 5.13. It is also easier to align 24 valleys with the bridges, since it is a multiple of 8. The amplitude is 0.35mm, even if it is hard to efficiently grind away that amount of material. An amplitude of 0.25mm is not enough to meet the requirements on stress and slip angle. The cutout has a length of 0.5mm with a depth of 0.1mm. The reason for not choosing a smaller cutout even if it gives a better result is that the manufacturing tolerances have a larger effect on a smaller cutout. The shaft's diameter is 55.5mm. A diameter of 50mm performed better when considering the stress, but the difference is small and a smaller shaft will increase the weight of the assembly. The grip for the chosen geometry will vary between 45µm and 105µm, since the largest grip is still able to be assembled when considering the required diametrical play of 0.040mm and heating rotor stack to 180°C and shaft to -40°C, as seen in Figure 5.7.

The slip angle, β, at 2.0Nm is 0.19°, which can be seen in Figure 6.1. This is a low value compared to the results for other valley geometries, but it is still much larger than the circular geometry with a grip of 110µm. Therefore the slip angle's impact on the efficiency needs to be evaluated. Still the value is below the maximum of 0.7° and hence the goal is considered to be achieved.

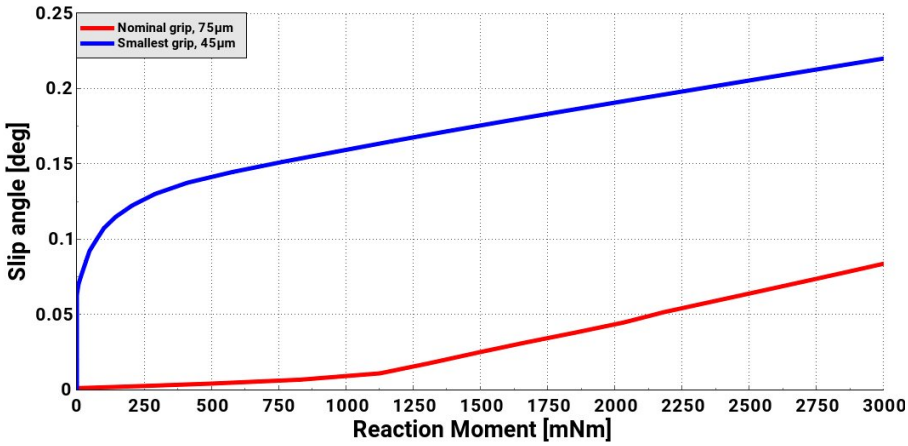

Figure 6.1: Slip angle for the final design versus reaction moment at different grips. The red curve represents the smallest grip and the blue the nominal grip. The simulations is carried out at 16300RPM.

Figure 6.2 shows the stress distribution around the shaft with the smallest grip of 45µm. This grip gives the highest stress due to the friction force being small and not absorbing much of the reaction moment, instead, most of the torque is being transferred by the valleys. The largest stress in this area is a compressive stress with a value of 301MPa, which is lower than the yield limit of 421MPa and therefore the goal are considered fulfilled.

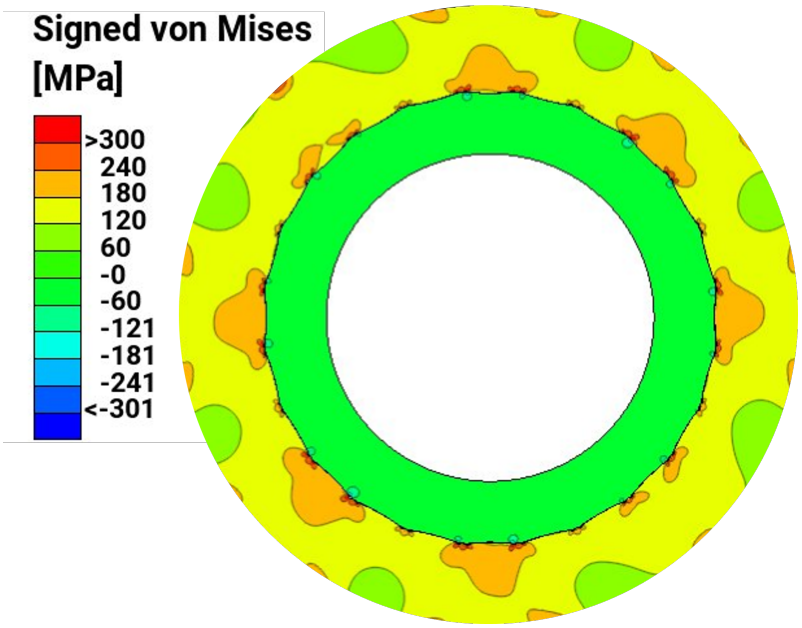

Figure 6.2: Plot of the stress distribution close to the valleys. The grip is the smallest grip of 45µm

7
Discussion and Future Work

The developed solution from the project has to be further evaluated and tested before it safely and reliably can be implemented in an electric machine. This chapter will present the future work needed to achieve this and relevant discussions.

7.1 Alternative boundary conditions

To obtain the results in terms of transferable torque and slip angle, different loads and boundaries were tested. The current solution is described in Section 3.3.2, but alternatives, such as fixating the outer edge of the laminate in the tangential direction and rotating the shaft were also tried out. The coupling was then attached from the center node to the inner edge of the shaft. This way of setting up the boundary conditions function very similar to the chosen method, but showed more inconsistent results. Another way to measure torque and angle which was evaluated is to fixate the shaft and applying a point load in tangential direction on every node on the outer edge of the laminate. This method does not always converge. The reason might be that the laminate slips too much from the shaft, and then there is no resistance against the applied load.

7.2 Evaluate efficiency loss

If the slip angle becomes larger, the machine's efficiency will decrease. The new efficiency needs to be evaluated to ensure that the new larger slip angle does not have a sufficient impact. This is not within the scope of this thesis, because the focus is only on the structural analysis of laminate and shaft.

7.3 Remodel of shrink fit

Smaller elements in the mesh make it possible to capture deformations and stresses with higher accuracy. The way that the shrink fit is modeled limits the minimum size of the elements at the contact, described in Section 3.3.1. If the contact is modeled in another way, it may be possible to use smaller elements around the interference. The results gained from the used method are sufficient for the purpose of the thesis, and changing it is probably only of interest if results from the simulation do not match real life tests.

7.4 Simulation of heating and cooling

The possible grip has been calculated from the analytical solution and could therefore be too conservative. Therefore, the heating and cooling process during assembly must be simulated since the results may show that it is possible to have a larger grip or larger amplitude of the valleys.

7.5 Temperature variations

The shaft is supposed to have oil running through it when in use, cooling down itself and the laminate. When driving, the electrical machine will heat up, causing it to expand which the oil is suppose to prevent. The flow of the oil inside the shaft is greatly dependent on the inner diameter of the shaft, but knowledge of how it is affected is missing. If only heating was applied to the assembly, some solutions might have been eliminated in the design process which in reality would have fulfilled the requirements, hence this is something that must evaluated in the future.

7.6 Fatigue analysis

Because of the changed geometry of shaft and laminate, new stress concentrations are introduced. The stresses are below but close to the yield limit at maximum RPM. To ensure a sufficient fatigue life for the laminates, a fatigue analysis needs to be evaluated. Predicting the fatigue life can be hard and sometimes too conservative results are obtained, therefore a fatigue test is also required. Though the maximum stress i close to the yield limit, it occurs when the machine is running at maximum velocity which it rarely does. The fatigue life should probably be evaluated during normal operating speeds, where the stresses are considerably lower.

7.7 Real life testing

To validate the model against real life test needs to be conducted, similar to the friction lock tests that has already been done. The testing should involve the following:

- Aligning shaft and rotor stack when performing the shrink fit
- Fixate shaft in torque machine while rotor stack is fixated in the lightening holes.
- Apply and measure torque from torque machine
- When torque request is met, measure slip angle

The critical grip that needs to be tested is the smallest of 45µm with an applied centrifugal force. Therefore, the actual grip that should be tested is smaller than 45µm.

Bibliography

[1] Volvo Personvagnar. Xc90 t8 twin engine – integrated electric drive unit, 2014.

[2] M. Gross. A planet with two billion cars. *Current Biology*, 26(8):R307–R310, 2016.

[3] S.N. Vukosavic. *Electrical Machines*. Power Electronics and Power Systems. Springer, 2012.

[4] J. Liang, J. Jiang, B. Bilgin, and A. Emadi. Shaft design for electric traction motors. *IEEE Transactions on Transportation Electrification*, 4(3):720–731, 2018.

[5] B. Bilgin, J.W. Jiang, and A. Emadi. *Switched Reluctance Motor Drives: Fundamentals to Applications*. CRC Press, 2019.

[6] A.O. Lebeck. *Principles and Design of Mechanical Face Seals*. A Wiley-Interscience publication. Wiley, 1992.

[7] A. P. Raj, A. Bhatti, and P.B. Dhanish. Combined effect of cylindricity, roundness and roughness on axial load-carrying ability of interference fits. *Proceedings of the Institution of Mechanical Engineers, Part J: Journal of Engineering Tribology*, 234:135065012091988, 04 2020.

[8] V. Vincenzo. *Circular Cylinders and Pressure Vessels. [electronic resource] : Stress Analysis and Design.* Springer Series in Solid and Structural Mechanics: 3. Springer International Publishing, 2014.

[9] M. Mägi, K. Melkersson, and M. Evertsson. *Maskinelement*. Studentlitteratur, 2017.

[10] A.C. Urgural and S.K. Fenster. *Advanced Mechanics of Materials and Applied Elasticity*. Pearson, 2012.

[11] C. Ding, X. Qi, Z. Gao, and L. Chang. The influence of centrifugal force on the interference fit of high-speed electric spindle. *World Journal of Engineering and Technology*, 8(4), 2020.

[12] J. Zhao, Wang J., Chao. Yu, Si-Q. Tang, and Jin Yao. Influence of radial interference on torque capacity of shrink-fit camshaft. *Advances in Mechanical Engineering*, 11, 2019.

[13] MATLAB. *9.7.0.1190202 (R2019b)*. The MathWorks Inc., Natick, Massachusetts, 2019.

[14] D. Wiley, H. Childs, B. Gregorski, B. Hamann, and K. Joy. Contouring curved quadratic elements. 01 2003.

[15] *ABAQUS Materials User's Guide, Version 2021*. Dassault Systemes Simulia Corp, United States, 2020.

[16] E. Weisstein. Ellipse. from mathworld–a wolfram web resource.

[17] E. Weisstein. Superellipse. from mathworld–a wolfram web resource.

[18] E. Weisstein. Squircle. from mathworld–a wolfram web resource.

A

Appendix

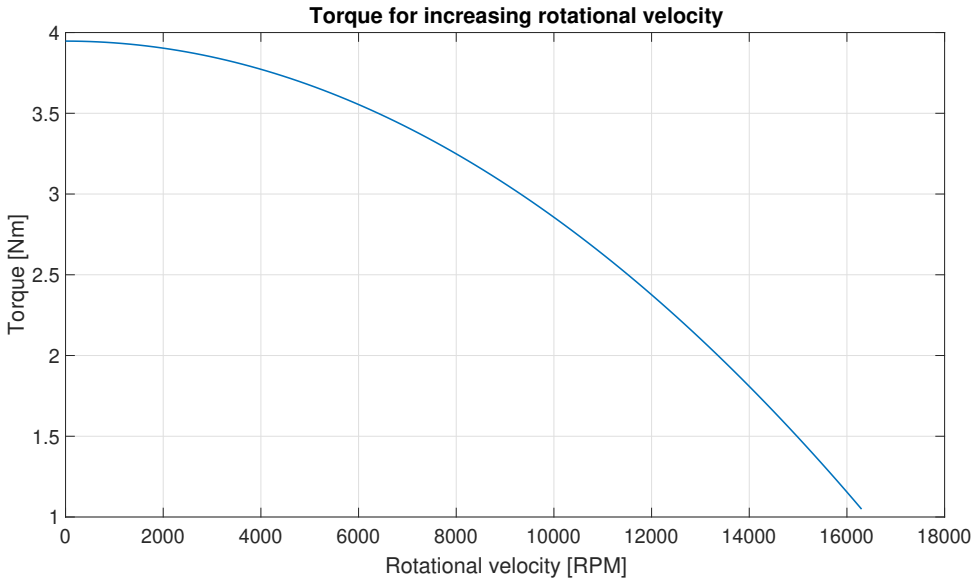

Figure A.1: Transferable torque with increasing rotational velocity using the grip $\Delta = 45\mu m$. At 16300RPM the torque which can be transferred is 1.05Nm.

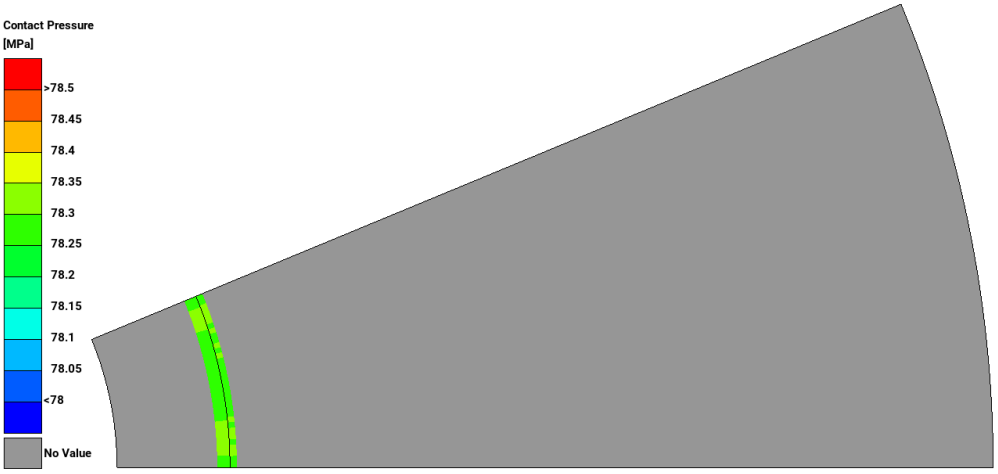

Figure A.2: Contact pressure, stationary case with diametrical grip $\Delta = 110\mu m$.

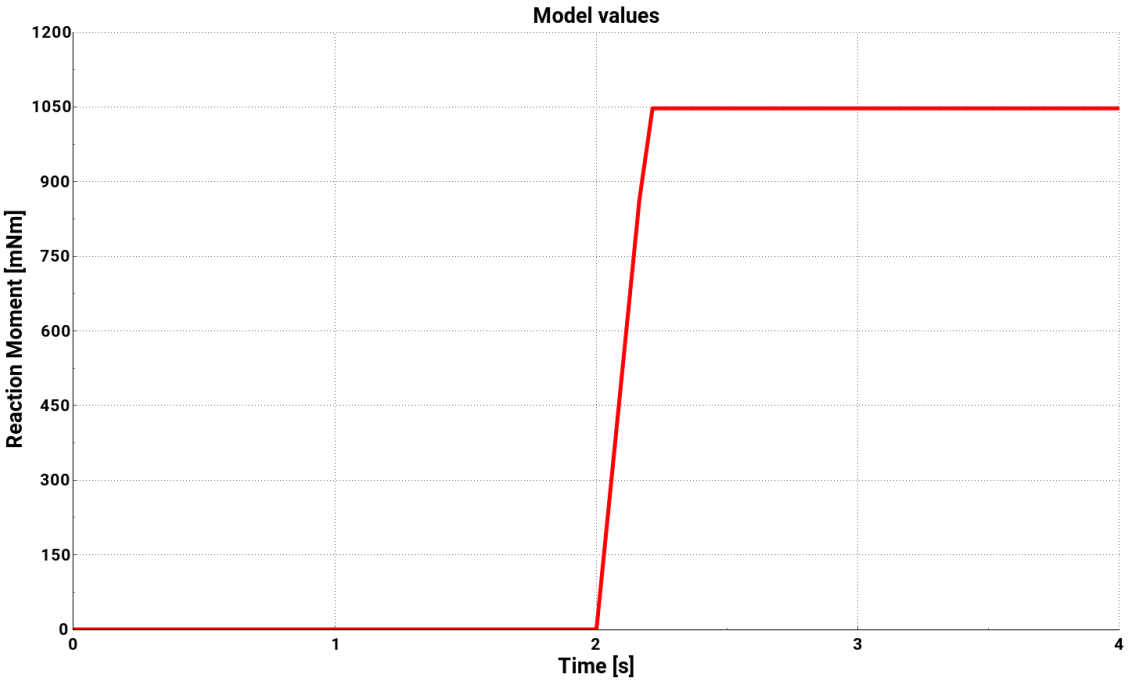

Figure A.3: Transferable torque at 16300RPM with the grip $\Delta = 45\mu m$. The rotor releases from the shaft at 1.05Nm.

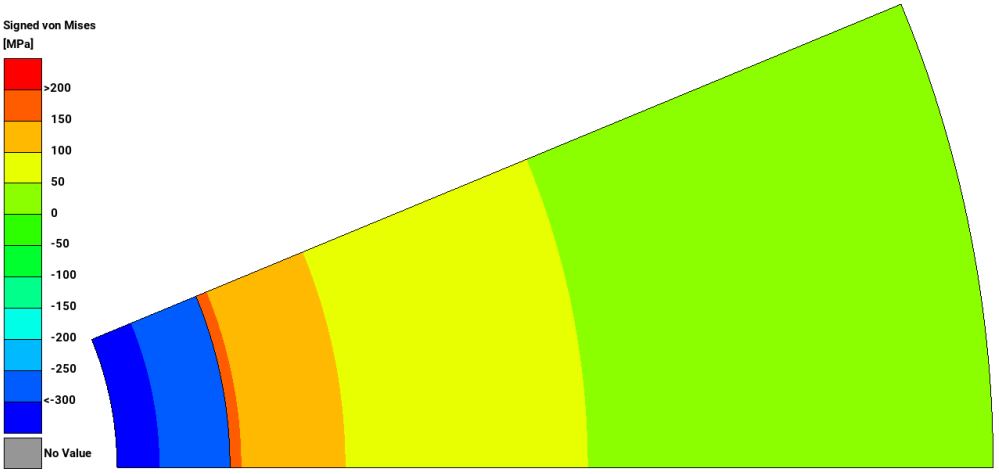

Figure A.4: Signed von Mises, stationary case with diametrical grip $\Delta = 110\mu m$.

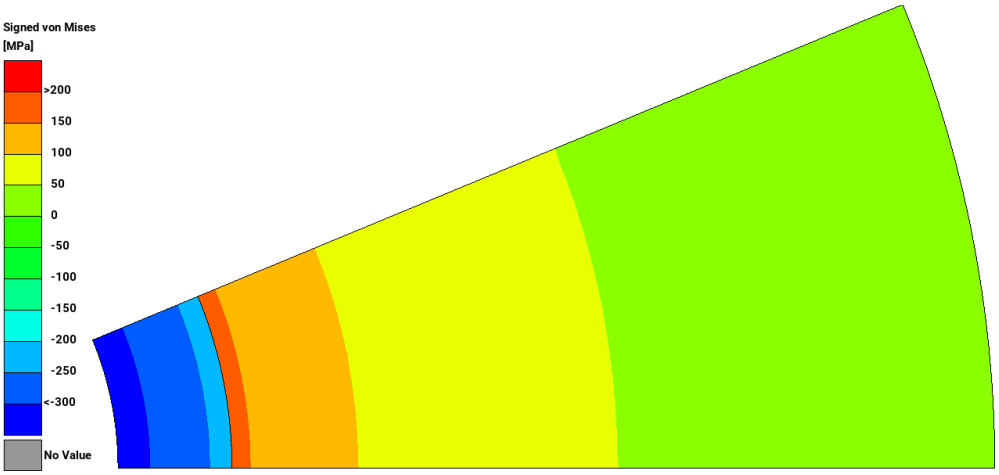

Figure A.5: Signed von Mises at 5000RPM with diametrical grip $\Delta = 110\mu m$.

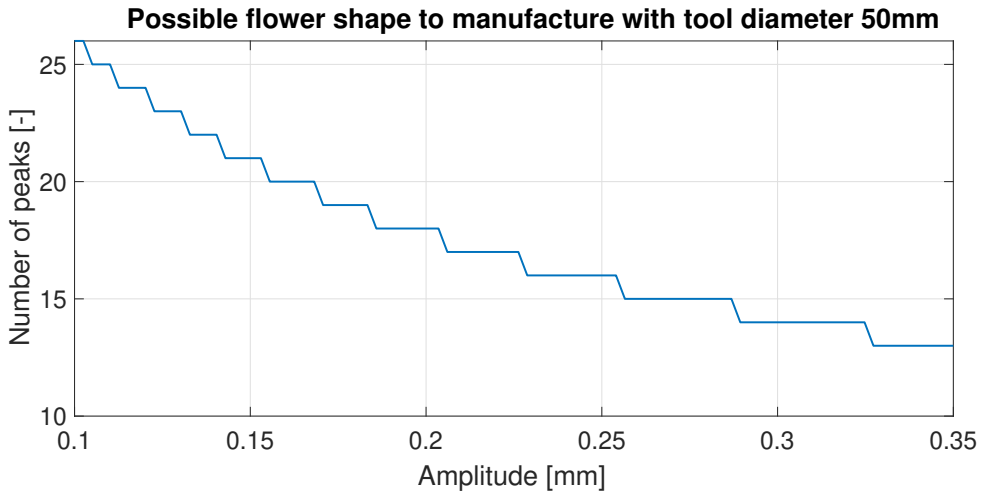

Figure A.6: Possible flower shape to manufacture with a tool diameter of 50mm. Shaft diameter is 55.5mm and the number of periods are plotted against the amplitude of them.

Figure A.7: Zoomed in image of sharp corner occurring when a valley is grinded into the shaft.

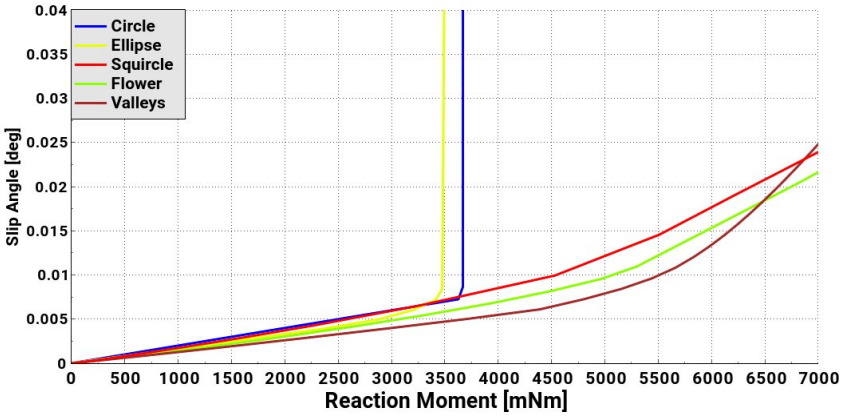

Figure A.8: Plot of slip angle versus reaction moment at 5000RPM for the different geometries

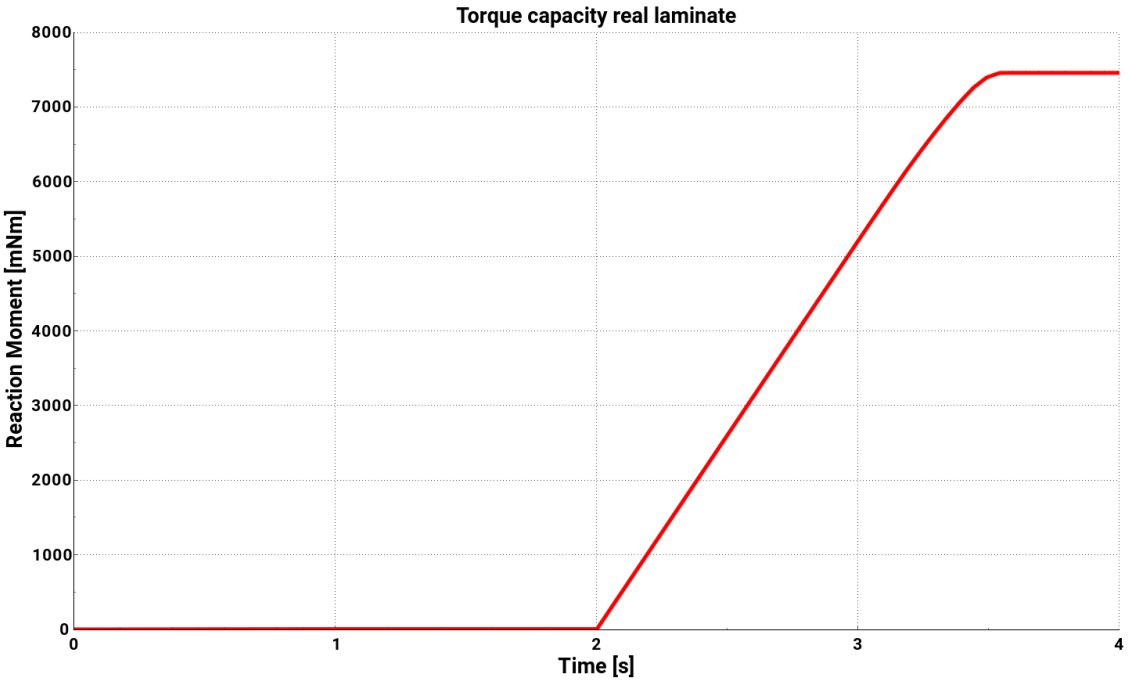

Figure A.9: Transferable torque for real laminate, stationary case with diametrical grip $\Delta = 110\mu m$.

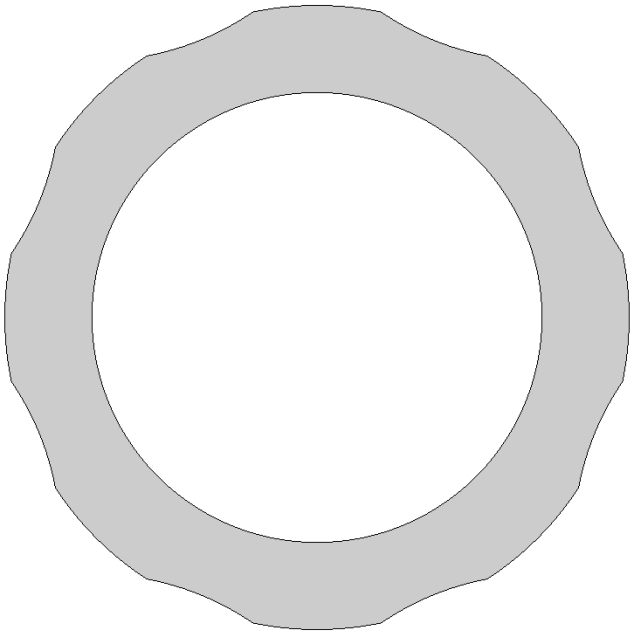

Figure A.10: The shape of shaft chosen to be optimized further. The geometry is exaggerated to better visualise the changes.

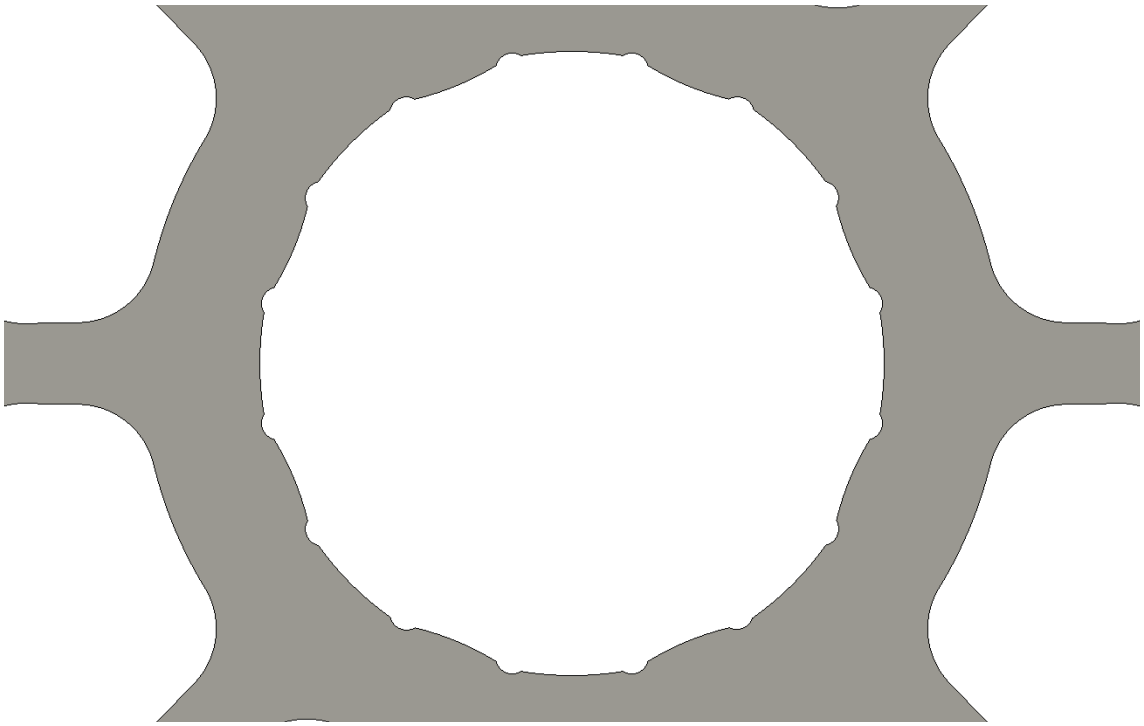

Figure A.11: Shape of the inner edge of the laminate chosen to be optimized further. The geometry is exaggerated to better visualise the changes.

Figure A.12: Close up of sharp corner and cutout made in laminate.

B

Appendix

Listing B.1: Script used to make changes of the geometry during the optimization process.

```
import numpy as np
import math
import ansa
from ansa import guitk
from ansa import constants
from ansa import base


#Create  window
def add_function_name():
  TopWindow = guitk.BCWindowCreate("DAN", guitk.constants.
   BCOnExitDestroy)
  BCHBox_1 = guitk.BCHBoxCreate(TopWindow)
  BCVBox_1 = guitk.BCVBoxCreate(BCHBox_1)
  BCVBox_2 = guitk.BCVBoxCreate(BCHBox_1)

  TxtDiameter = guitk.BCLabelCreate(BCVBox_1, "Diameter")
  TxtAmplitude = guitk.BCLabelCreate(BCVBox_1, "Amplitude")
  TxtNumber = guitk.BCLabelCreate(BCVBox_1, "Number")

  InputDiameter = guitk.BCLineEditCreateDouble(BCVBox_2, 55.5)
  InputAmp = guitk.BCLineEditCreateDouble(BCVBox_2, 0.25)
  InputNumber = guitk.BCLineEditCreateInt(BCVBox_2, 16)


  BCDialogButtonBox_1 = guitk.BCDialogButtonBoxCreate(TopWindow)
  guitk.BCWindowSetAcceptFunction(TopWindow, _ok_pressed, [
   InputDiameter, InputAmp, InputNumber])

  guitk.BCShow(TopWindow)

def _ok_pressed(w,data):
  diameter =  guitk.BCLineEditGetDouble(data[0])
  amp = guitk.BCLineEditGetDouble(data[1])
  number = guitk.BCLineEditGetInt(data[2])

  _generate_geometry(diameter, amp,number)
  return True

def _generate_geometry(diameter, amp, number):
  ProjectGeometry(diameter, amp, number)
  ChangePID()
  return True

def ChangePID():

  LamCutFace = base.GetEntity(constants.ABAQUS,"FACE",35)
  lamBounds = base.DefineInterfaceBoundary(LamCutFace,  red = True)
  for i in range (36,100):
    v = base.GetEntity(constants.ABAQUS, "FACE", i)
```

```
49      p_prop_old = base.GetEntity(constants.ABAQUS,"SHELL_SECTION",
        2)
50      p_prop_new = base.GetEntity(constants.ABAQUS, "SHELL_SECTION",
        1)
51      s = base.ReplaceProperty(p_prop_old,p_prop_new,v)
52      cutBounds = base.DefineInterfaceBoundary(v, red=True)
53      status = base.SmartPaste(lamBounds,cutBounds)
54      print(s)
55
56
57
58    print(lamBounds)
59
60
61    return True
62
63  def ProjectGeometry(d,a,n):
64    #file  = '/vcc/cae/backup/edl/STRUC/User/enyland2/Matlab/
        Manufacturing/FlowerNoPeaks.csv'
65    r = d/2
66    Rt = 27.5
67
68    ang = np.linspace(0,math.pi*2,n+1)
69
70    # Polar coordinates
71    r1 = r + Rt-a
72
73    # Cartesian coordinates
74    xCart1 = r1 * np.cos(ang)
75    yCart1 = r1 * np.sin(ang)
76
77    for i in range(len(xCart1)):
78      point1 = base.Newpoint(xCart1[i],yCart1[i],0)
79      Curve = base.CreateCircleCenter2PointsRadius( [xCart1[i],yCart1
        [i],0],[1,0,0], [0,1,0], 27.5)
80
81    Shaft = base.GetEntity(constants.ABAQUS,"FACE",1)
82    Curves = base.CollectEntities(constants.ABAQUS,None,"CURVE")
83    ret_list = base.ConsProject(entities=Curves,faces_array=Shaft,
        connect_with_faces=True)
84    newFaces = ret_list[1]
85    base.DeleteFaces(newFaces)
86    #base.DeleteCurves('all', True)
87    return point1
88
89  add_function_name()
```

DEPARTMENT OF INDUSTRIAL AND MATERIALS SCIENCE
CHALMERS UNIVERSITY OF TECHNOLOGY
Gothenburg, Sweden
www.chalmers.se

CHALMERS
UNIVERSITY OF TECHNOLOGY